Understanding Mid-Latitude Jet Variability and Change using Rossby Wave Chromatography: Wave-Mean Flow Interaction

DAVID J. LORENZ *

Center for Climatic Research, University of Wisconsin-Madison, Madison, WI

ABSTRACT

Rossby Wave Chromatography (RWC) is implemented in a linearized barotropic model as a tool to understand the interaction between the mid-latitude jet and the eddy momentum fluxes (UV) in an idealized GCM. Given the background zonal-mean flow and the space-time structure of the baroclinic wave activity source, RWC calculates the space-time structure of the upper tropospheric UV. RWC allows a clean separation of the effects of phase speed changes and index of refraction changes on UV. It is found that UV reinforces imposed zonal-mean zonal wind (U) anomalies that are collocated with the centers of action of EOF1 of the GCM. Critical level dynamics are essential for the positive feedback when U is equatorward of the mean jet and "reflecting level" dynamics are essential for the positive feedback when U is poleward of the jet. The UV caused by changes in the phase speeds of the wave sources, on the other hand, are associated with a negative feedback. When the imposed U is out of phase with EOF1, the eddies tend to shift the imposed U poleward (equatorward) for anomalies that are equatorward (poleward) of the poleward center of action of EOF1. Critical (reflecting) level dynamics is most important for the poleward shift in the subtropics (mid-latitudes). Because there are no baroclinic feedbacks in these experiments, these results suggest that barotropic feedbacks alone can account for the structure of the U variability in the mid-latitudes.

1. Introduction

This is the final paper of a three part series on the use of Rossby Wave Chromatography (Held and Phillips (1987); Lorenz (2014a); Lorenz (2014b)) to understand the response of the mid-latitude jet to external forcing and, in this paper in particular, the internal variability of the mid-latitude jet. By Rossby Wave Chromatography (RWC), we mean that we calculate the space-time (i.e. phase speed-latitude-wavenumber) structure of the upper tropospheric eddy momentum fluxes given the background zonal-mean flow and the space-time structure of the baroclinic wave activity source (convergence of vertical EP flux in the upper troposphere) (Held and Hoskins (1985); Held and Phillips (1987); Randel and Held (1991)). The dynamics of the eddies in our implementation of RWC are governed by the linearized barotropic vorticity equation on a sphere. Unlike other studies of the forced barotropic vorticity equation (Vallis et al. (2004); Barnes et al. (2010); Barnes and Hartmann (2011); Kidston and Vallis (2012)), which specify the vorticity forcing directly, we specify the baroclinic wave activity source and find the forcing that is consistent with the wave source. In our barotropic model, the wave activity source is set equal to the convergence of the vertical EP flux averaged over the upper troposphere in a GCM and the background zonal-mean zonal wind and absolute vorticity gradients are weighted vertical averages of the zonal-mean zonal wind and absolute vorticity gradients in the GCM. In Lorenz (2014a), we show that the RWC model can simulate the important features of the GCM's internal variability and its response to external forcing.

In our implementation of RWC, the wave activity source and the background flow are prescribed independently, so that one can change the wave activity source while keeping the background winds and vorticity gradients constant. Similarly, one can change the background

* *Corresponding author address:* David J. Lorenz, Center for Climatic Research, University of Wisconsin-Madison, 1225 W. Dayton St., Madison, WI 53706.
E-mail: dlorenz@wisc.edu

winds and vorticity gradients while keeping the wave activity source constant. We call the latter experiment the response to changes in Index Of Refraction (IOR). One can also increase the phase speeds of the wave activity source, for example, while also keeping the magnitude of the wave activity source integrated over phase speed constant. We call this experiment the response to changes in the phase speed of the wave activity source. Such perturbations to the RWC model are useful for understanding the dynamics because linear superposition nearly holds: the sum of the response with only the wave activity source altered and the response with only the background flow altered is equal to the response with both perturbations applied together (Lorenz (2014b)). With complete freedom to perturb the various components of the full response, we can identify the dynamical mechanisms responsible for changing the latitude of the jet in response to external forcing and the dynamical mechanisms responsible for selecting the leading "modes" of the jet's internal variability.

In Lorenz (2014b), we explored the mechanisms responsible for *maintaining* poleward shifted jets in response to external forcing that acts to make the jet stronger. We found that changes in the IOR are responsible for maintaining the poleward shifted jet via changes in wave reflection (Kidston and Vallis (2012)). In the control climate there exists a selective "reflecting level" (or turning latitude) on poleward flank of jet: for a given wavenumber, low phase speed waves are reflected but high phase speed waves are absorbed at the critical level on the poleward flank of jet (Fig 1a, the arrows represent the horizontal wave activity flux, $F_y = -\overline{u'v'}\cos\phi$, where ϕ is the latitude). When the zonal-mean zonal wind increases on the poleward flank of the jet, the peak of the reflecting level extends to higher phase speeds and a wider range of poleward propagating waves encounter a reflecting level instead of a critical level on the poleward flank (Fig 1b, to focus attention on the essential dynamics, only the reflecting level changes in the schematic) (Kidston and Vallis (2012)). The increased wave reflection leads to increased equatorward propagating waves (and therefore poleward momentum flux) across the jet. The equation governing the phase speed of the reflecting level is simply the Rossby wave dispersion relation with the meridional wavenumber set to zero:

$$c_\omega = \frac{\bar{u}}{a\cos\phi} - \frac{\beta^* a\cos\phi}{m^2}, \qquad (1)$$

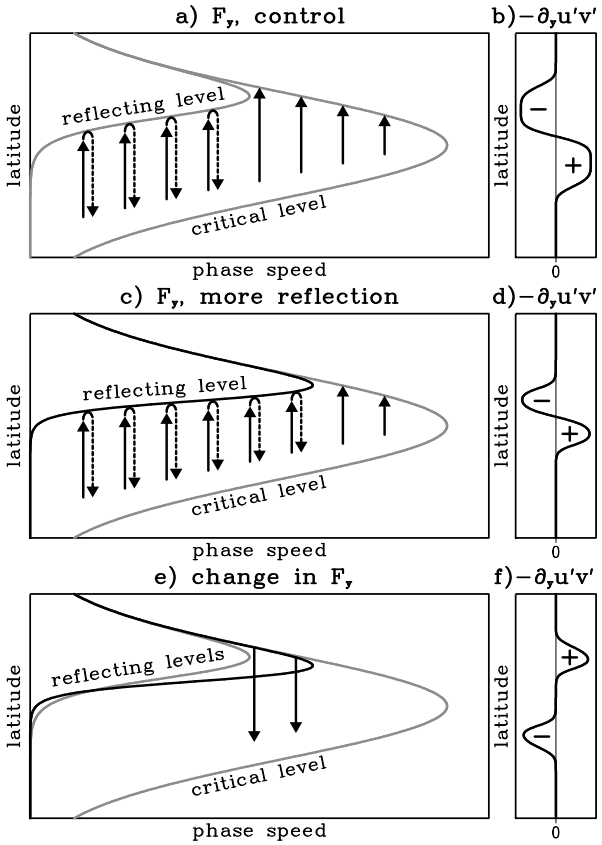

Figure 1: Schematic of the effect of the reflecting level on wave activity fluxes, F_y, in latitude/phase speed space (a,c,e) and the momentum flux convergence (integrated over phase speed) associated with these wave activity fluxes (b,d,f). The arrows point in the direction of the wave activity flux, which is *opposite* the momentum flux. The schematic *only* shows waves that initially propagate poleward. Reflected waves are dashed. The critical and reflecting levels are labeled. Note this schematic represents a single zonal wavenumber since the reflecting level is wavenumber dependent. a) Control F_y. b) Control momentum flux convergence integrated over phase speed. c) F_y for a state with more reflection. Note that the peak in the reflecting level extends to higher phase speeds. d) Momentum flux convergence for a state with more reflection. e) Solid arrows: net change in F_y. f) Net change in momentum flux convergence.

where c_ω is the angular phase speed, $\bar{u}$ is the zonal-mean zonal wind, a is the radius of the earth, β^* is the absolute vorticity gradient ($= a^{-1}\partial_\phi(f + \bar{\zeta})$, where f is the Coriolis parameter and $\bar{\zeta}$ is the zonal-mean relative vorticity) and m is the *integer* zonal wavenumber. The reflecting level is most important on poleward flank of the jet because it extends to the highest values of c_ω there. The maximum c_ω is on the poleward flank because 1) the planetary portion of β^* goes to zero toward the pole and 2) the relative vorticity gradient is proportional to minus the second derivative of $\bar{u}$, which means that the circu-

lation induced portion of β^* is smallest on the jet flanks and largest in the jet core. Both these effects decrease β^* on the poleward flank and by (1) imply that the maximum (in c_ω) of the reflecting level is on the poleward flank. Equation (1) also implies that increases in $\bar{u}$ on the poleward flank lead to more reflection while increases in β^* on the poleward flank lead to less reflection. RWC experiments in Lorenz (2014b) support this inference.

The presence of a selective reflecting level on the poleward flank of the jet also has important consequences for the response to changes in phase speed of the wave activity sources (Lorenz (2014b)). In the literature, ideas on the effect of phase speed changes on momentum fluxes emphasize the equatorward propagating waves and the critical level on the equatorward flank (Chen et al. (2007)). The relevant fluxes of wave activity in the control climate look like Fig. 2a. An increase in wave phase speeds means the spectrum shifts to the right leading to increased (decreased) equatorward propagating waves at high (low) phase speeds (Fig. 2b). In shifting to the right, the waves are still constrained to stop at their critical latitude, which they reach slightly sooner compared to the control case. Therefore, there is a net decrease in equatorward wave activity at all latitudes where there is a critical latitude for the waves. This leads to negative $\bar{u}$ forcing directly equatorward of the jet and positive forcing deeper in the subtropics as described in Chen et al. (2007) (Fig. 2d). In the presence of a selective reflecting level, however, higher phase speeds also imply more wave absorption and less wave reflection on the poleward flank of the jet (Fig. 2c). The net result is a reduction in momentum fluxes across the jet in addition to the reduction on the equatorward flank. Hence increases in phase speed actually oppose the poleward shift (Lorenz (2014b)).

The changes in IOR and the increase in phase speeds impact wave reflection in opposite ways. In Lorenz (2014b), we found that the IOR changes are more important, leading to increased reflection and positive momentum fluxes across the jet. In order to understand the relative importance of $\bar{u}$ and phase speed changes we need to better understand how the wave source phase speeds change relative to the reflecting level. Kidston et al. (2011) suggest that the horizontal scale of the waves increases as the jet shifts poleward. Increases in wave scale imply that wave phase speeds will decrease *relative* to $\bar{u}$, which is in the correct direction to explain the dominance of IOR over phase speed. In Lorenz (2014a), however, we find that changes in wave scale are either very weak or essentially nonexistent among the GCM runs we considered, yet all runs showed a pronounced poleward shift of the jet. An alternative explanation for the dominance of IOR over phase speed changes is presented below.

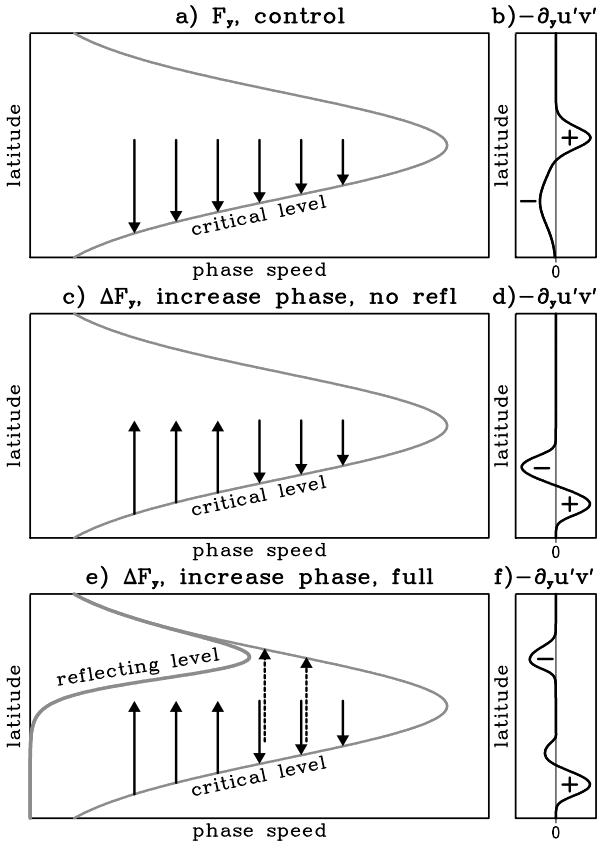

Figure 2: Schematic of the effect of changes in wave activity source phase speeds on wave activity fluxes, F_y, in latitude/phase speed space (a,c,e) and the momentum flux convergence (integrated over phase speed) associated with these wave activity fluxes (b,d,f). The arrows point in the direction of the wave activity flux, which is *opposite* the momentum flux. The critical and/or reflecting levels are labeled. a) F_y in a control run where only initially equatorward propagating waves are considered. b) Momentum flux convergence integrated over phase speed where only initially equatorward propagating waves are considered. c) The change in F_y in response to increases in phase speed where only initially equatorward propagating waves are considered. d) The change in momentum flux convergence in response to increases in phase speed where only initially equatorward propagating waves are considered. e) The full change in F_y in response to increases in phase speed. Higher phase speeds mean that poleward propagating waves near the peak of the reflecting level that were once reflected are now absorbed at the critical level on the poleward flank of the jet. The net effect is the response in (c) *minus* the response in Fig. 1e. Note this plot represents a single zonal wavenumber since the reflecting level is wavenumber dependent. f) The net momentum flux convergence associated with (e).

In this paper, we will investigate the response of the RWC model to prescribed $\bar{u}$ anomalies and the response when the RWC model is coupled to a simple barotropic $\bar{u}$ model where the $\bar{u}$ tendency is simply the sum of the eddy momentum flux convergence and a Rayleigh damping term acting on $\bar{u}$. In addition to providing a better understanding of the response to external forcing, this analysis will enhance our understanding of the mechanisms that determine the "modes" of internal variability, given that a long-term positive feedback between $\bar{u}$ anomalies and the eddy momentum fluxes select the leading EOF (Lorenz and Hartmann (2001); Lorenz and Hartmann (2003)). The proposed mechanisms for the positive feedback between $\bar{u}$ and the eddies fall into two general categories: "baroclinic mechanisms" that depend on changes in the baroclinic wave activity source (Robinson (1996); Robinson (2000); Lorenz and Hartmann (2001); Chen and Plumb (2009); Rivière (2009); Zhang et al. (2012)) and "barotropic mechanisms" that depend on changes in meridional wave propagation independent of changes in the baroclinic wave source (Hartmann (1995); Hartmann and Zuercher (1998); Jin et al. (2006a); Jin et al. (2006b); Chen and Zurita-Gotor (2008); Barnes et al. (2010); Barnes and Hartmann (2011)). In addition to the positive feedback between EOF1 and the eddies, other feedbacks lead to the poleward and equatorward propagation of $\bar{u}$ anomalies (James and Dodd (1996); Feldstein (1998); Lee et al. (2007); Sparrow et al. (2009)).

In this paper, we explore the response of the eddies to small $\bar{u}$ perturbations about the Held and Suarez (1994) basic state. The effect of $\bar{u}$ on the eddies is calculated using RWC and a simple model of the phase speeds of the wave activity source (see Lorenz (2014a)). We only consider wave-mean flow interaction for the case where the latitudinal profile of the baroclinic wave activity flux is constant because, as shown in Lorenz (2014a), barotropic processes appear to explain much of the structure and evolution of $\bar{u}$ anomalies. Baroclinic feedbacks will be considered in future work. We begin this paper with a brief description of the GCM and the RWC model. In section 3, we explore the RWC response as a function of the latitude of imposed $\bar{u}$ anomalies. In section 4, we isolate and understand the dynamical mechanisms involved in section 3. Next, we briefly discuss the RWC response as a function of the width of imposed $\bar{u}$ anomalies (section 5). Finally, we discuss the modifications to the above picture when the eddies and $\bar{u}$ are fully coupled (section 6).

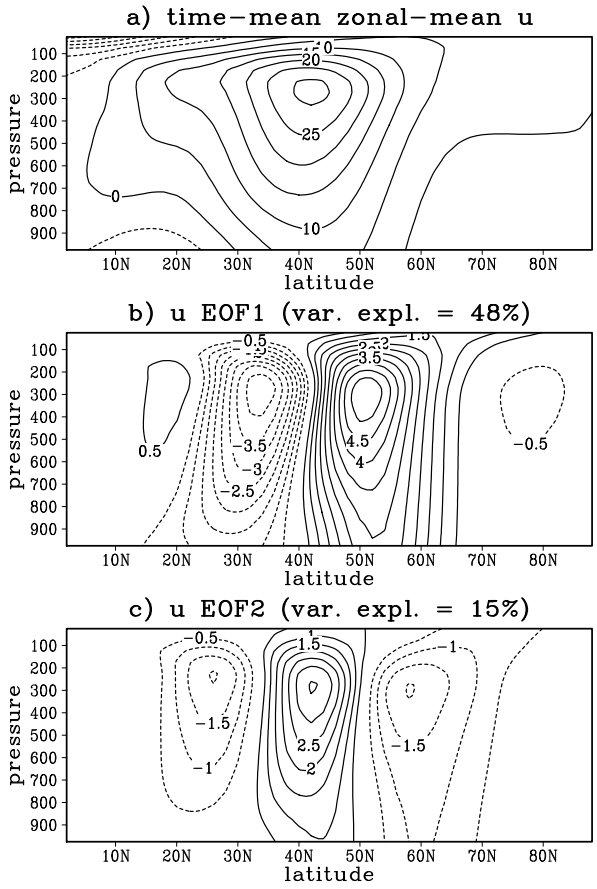

Figure 3: a) The time-mean zonal-mean zonal wind in the control run (m s^{-1}). b) EOF1 of the zonal-mean zonal wind as represented by the regression of the zonal-mean zonal wind anomalies on the first principal component (m s^{-1}). c) Same as (b) but for EOF2.

2. GCM and RWC model

The dynamical core of the GCM is described in Lorenz (2014a) and all details regarding resolution and integration length can be found there. The standard idealized forcing given in Held and Suarez (1994) is used as the control run. The time-mean zonal-mean zonal winds for the control experiment are shown in Fig. 3a. The latitude of the mid-latitude jet is 42° and there is a shoulder of strong $\bar{u}$ extending into the subtropics associated with the subtropical jet. The first two EOFs of the instantaneous (i.e. not monthly averaged) $\bar{u}$ variability are shown in Figs. 3bc. The leading EOF has opposite polarity anomalies on either side of the mean mid-latitude jet and therefore represents north/south shifts in the jet. The second EOF represents a strengthening and narrowing of the jet in one phase and a weakening and broadening of the jet in the opposite phase. Similar mean jet and

EOF patterns are present in observations of the Southern Hemisphere (Lorenz and Hartmann (2001)). The focus of this paper is on diagnosing the response of the RWC model to perturbations about a control $\bar{u}$ and wave activity source spectrum (both taken from the GCM) in order to understand the eddy feedbacks associated with these EOF structures. For more comparisons between the RWC model and the GCM see Lorenz (2014a).

RWC calculates eddy momentum fluxes from the background $\bar{u}$ and the wave activity source spectrum. Prescribing the wave source spectrum essentially amounts to prescribing the covariance between the vorticity and the vorticity forcing for each wavenumber and phase speed under the assumption that the vorticity is related to the forcing by the linearized barotropic vorticity equation on a sphere (see Lorenz (2014a)). The wave activity source spectrum is defined as the convergence of the vertical EP flux (Edmon et al. (1980)) averaged from $\sigma = 0.125$ to $\sigma = 0.525$. The eddy momentum fluxes calculated from RWC are intended to simulate the GCM eddy momentum fluxes averaged over the same σ-level range. The RWC response is defined as the change in eddy momentum fluxes from the RWC simulation with perturbed $\bar{u}$ and wave activity source spectrum minus the RWC simulation with control inputs. To apply a barotropic model of the eddies to diagnose the multi-level GCM, we must prescribe a single level background zonal wind and absolute vorticity field. To this end, we calculate the vertical Empirical Orthogonal Functions (EOFs) of the eddy ψ over longitude and time for each latitude. The values of the first ψ EOF define the relative weights for averaging the multi-level zonal-mean zonal wind ($\bar{u}$) and β^* ($= a^{-1}\partial_\phi(f + \bar{\zeta})$ where ϕ is the latitude) into a single number for each latitude (see Lorenz (2014a)). This vertical weighted average is applied any time a diagnostic or model requires a barotropic $\bar{u}$ (i.e. involves a single vertical level).

For an example of the application of RWC to the control run of the GCM see Figs. 4abc. The wave source spectrum (Fig. 4a) and the background $\bar{u}$ and β^* (Fig. 4b) are the inputs to the RWC model. From these, the RWC method predicts the eddy momentum flux spectrum (Fig. 4c). Note the spectra in Figs. 4ac are summed over m. The actual RWC calculations are performed individually to each m and c_ω in the spectrum (the background flow is steady and zonally symmetric so each m and c_ω are decoupled).

Because the RWC model requires the wave activity source spectrum as input and the effect of the wave source changes on the eddy momentum fluxes is not negligible (see Lorenz (2014b)), we need to be able to model the changes in the wave source given the background flow. In this paper, we use the simple model of the changes in the phase speeds of the source described in Lorenz (2014a). The model is based on the barotropic dispersion relation:

$$c_\omega = \frac{\bar{u}}{a\cos\phi} - \frac{\beta^* a\cos\phi}{m^2 + l^2}, \tag{2}$$

where l is the meridional wave number. Lorenz (2014a) assumes that the changes in the horizontal wavenumber are small (i.e. m^2+l^2 is constant) so that the phase speed in a perturbed state (subscript 2) can be related to that in the control (subscript 1) by:

$$c_{\omega 2} = \frac{\bar{u}_2}{a\cos\phi} + \frac{\beta_2^*}{\beta_1^*}\left(c_{\omega 1} - \frac{\bar{u}_1}{a\cos\phi}\right). \tag{3}$$

Lorenz (2014a) found that the actual wave source phase speed changes appear to be smoothed in latitude relative to predictions based on the dispersion relation. Therefore, for the simple model of the phase speed change, $\bar{u}_1$, $\bar{u}_2$, β_1^* and β_2^* are first smoothed in latitude with a Gaussian kernel, $\exp(-\phi^2/a_c^2)$, where a_c is 17° latitude, before applying (3). The predicted phase speed change is then used to shift the phase speed spectrum of the control run in a conservative way by mapping the power in each phase speed bin to the two bins closest to the new predicted phase speed. Lorenz (2014a) find that the simple model does a good job predicting the magnitude and structure of the phase speed changes in the response to external forcing in a GCM.

One unsatisfactory aspect of this simple model is the arbitrary smoothing parameter, a_c. While this smoothing parameter impacts the wave source phase speed changes, we will see below that this smoothing parameter has amazingly little impact on the momentum fluxes when we use these predicted wave sources to force the RWC model. Also, we consider only the phase speed changes in this paper because the focus is on the simpler case of nearly barotropic anomalies. Based on the results in Lorenz (2014a), we believe that to first order the dynamics related to mechanical forcing and the internal variability can be described without considering changes in the wave activity source integrated over phase (i.e. the baroclinic feedback). In future work, we will couple the

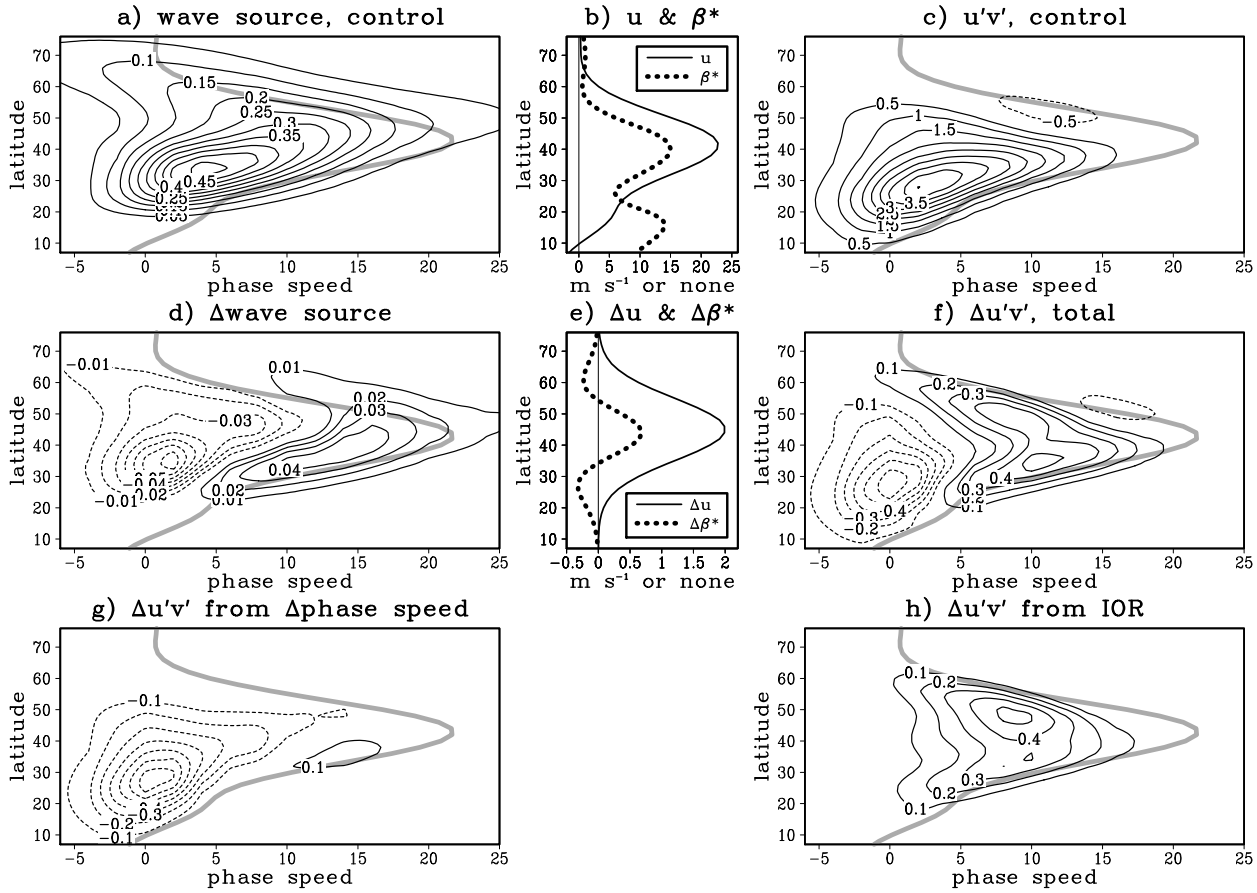

Figure 4: a) Latitude/phase speed spectrum of the vertical component of EP flux averaged from $\sigma = 0.125$ to 0.525 in the GCM in the control run (day^{-1}). The gray line is the critical level. The x-axis is angular phase speed in m s^{-1} at 45° (see section 2). b) A weighted vertical average of the zonal-mean zonal wind in the control run (thin solid) (m s^{-1}) and a weighted vertical average of the zonal-mean absolute vorticity gradient (thick dotted) non-dimensionalized by the radius of the earth and the length of day and multiplied by $\cos\phi$. c) Latitude/phase speed spectrum of the RWC eddy momentum flux calculated from (a) and (b) (m s^{-1}). d) As in (a) but for the change predicted by the phase speed model for the zonal-mean zonal wind perturbation in (e). e) As in (b) but for the perturbation applied to the control run. f) The change in the latitude/phase speed spectrum of the RWC eddy momentum flux from the perturbations in (d) and (e) (m s^{-1}). g) As in (f) but from the perturbed wave source (d) and the control background state (b) (m s^{-1}). h) As in (f) but from the control wave source (a) and the perturbed background state (e) (m s^{-1}).

RWC model to the zonal-mean circulation in the latitude-pressure plane and consider the effects of changes in the latitudinal profile of the source.

The RWC and phase speed models described above provide the eddy momentum flux given the wave source spectrum in the control run and the background zonal-mean zonal wind. In the full GCM, the resulting eddy momentum fluxes change the zonal-mean zonal wind, which then feeds back onto the eddies. To capture this effect, we coupled the RWC and phase speed models to a one layer version of $\bar{u}$:

$$\frac{dz}{dt} = \alpha h - \frac{z}{\tau} + F_z, \tag{4}$$

where z is the modelled one-layer $\bar{u}$ anomaly, h is the eddy vorticity flux anomaly in the RWC model when z is added to the climatological background wind, α and τ are constants that need to be determined and F_z is any imposed external forcing. The parameters α (= 0.59) and τ (= 9.07 days) are calculated using the relationship between the z and h in the internal variability in the control run of the GCM (Lorenz (2014a)). The coupled RWC model is integrated forward in time using simple forward differencing with an 8 hour time step as in Lorenz (2014a).

The angular phase-speed spectra (e.g. Randel and Held (1991)) are calculated as in Lorenz (2014a). For all figures in this paper, angular phase speed is given in

terms of velocity at 45° latitude in m s^{-1}. In other words, our angular phase speed (c) is related to the angular phase speed in rad s^{-1} (c_ω) by $c = c_\omega a \cos(45°)$, where a is the radius of the earth. The resolution in phase speed for all analysis and figures is 2 m s^{-1}.

3. Response as a function of zonal wind latitude

In this section, we show results from a series of RWC experiments with imposed $\bar{u}$ anomalies and we explore how the resulting $\overline{u'v'}$ anomalies feedback onto the imposed $\bar{u}$ anomalies. In particular, we quantify the degree of positive feedback and/or poleward/equatorward propagation as a function of the latitude of the imposed $\bar{u}$ anomaly.

First we show an example of the RWC response to an imposed $\bar{u}$ anomaly of the form $2\exp\left(-((\phi-\phi_0)/14°)^2\right)$ m s^{-1}, where $\phi_0 = 45°$ (Fig. 4e). This anomaly is the same width as the time mean jet. The change in the wave source spectrum from the phase speed model (Fig. 4d) represents a shift in the mean phase speed spectrum (Fig. 4a) to higher phase speeds. The associated change in the eddy momentum flux spectrum from the RWC model also shows a shift toward higher phase speeds, as well as increases on the poleward flank of the jet (Fig. 4f). Because the wave source spectrum and the background flow are prescribed independently, we can isolate their contributions by applying the wave source changes while holding the background flow constant (Fig. 4g), or vice versa (Fig. 4h). We immediately see that the apparent shift in the eddy momentum flux in Fig. 4f is only partially explained by the shift in the wave source spectrum. The sensitivity of reflection on the poleward flank of the jet to the phase speed of the incipient waves is the source of this paradox as discussed in the Introduction and in Lorenz (2014b). The IOR response (i.e. change background flow with no change in wave source phase speeds) shows a broad increase in the momentum flux (Fig. 4h). This response is a mixture of the reflecting level mechanism on the poleward flank (see Introduction and Lorenz (2014b)) and changes in the position of the subtropical critical level on the equatorward flank, which is explored in more detail below. Integrated over phase speed, the imposed positive $\bar{u}$ anomaly leads to positive $\overline{u'v'}$ changes due to IOR and negative $\overline{u'v'}$ due to changes in wave source phase speeds. When the sign of the $\bar{u}$ anomaly is reversed, the $\overline{u'v'}$ changes are also reversed (not shown). We will see below that for positive $\bar{u}$ anomalies of this meridional scale, the IOR changes are dominated by positive $\overline{u'v'}$ and the source phase speed changes are dominated by negative $\overline{u'v'}$ regardless of the latitude of the imposed $\bar{u}$ anomaly.

In Fig. 5, we repeat the above experiments for a large number of imposed $\bar{u}$ anomalies of the form $2\exp\left(-((\phi-\phi_0)/14°)^2\right)$ m s^{-1}. In these experiments the latitude of the maximum $\bar{u}$ anomaly, ϕ_0, varies in increments of 2° from the equator to the pole. The latitudinal profile of the $\overline{u'v'}$ response (integrated over phase speed and wavenumber) is shown on the x-axis, ϕ_0 is shown on the y-axis, and the gray line is the line $y = x$. The total $\overline{u'v'}$ response tends to be concentrated in two main latitude bands centered at 22° and 42° (Fig. 5a). When ϕ_0 is equatorward (poleward) of 38°, the 22° anomalies are positive (negative) and the 42° anomalies are negative (positive). The climatological jet is at 42° (Fig. 3a).

In Figs. 5b and 5c, we separate the effects of IOR changes and the effects of phase speed changes on the $\overline{u'v'}$ response. While the total $\overline{u'v'}$ is somewhat symmetric about $\phi_0 = 38°$, the IOR $\overline{u'v'}$ is instead dominated by positive anomalies in two separate latitude bands. The responses in these two bands do not occur together, instead the subtropical $\overline{u'v'}$ are "excited" when $\bar{u}$ is (approximately) equatorward of the mean jet (= 42°) and the mid-latitude $\overline{u'v'}$ are "excited" when $\bar{u}$ is poleward of the mean jet. The phase speed induced $\overline{u'v'}$, on the other hand, are broad and negative regardless of the location of the imposed $\bar{u}$ anomalies. Therefore, the total $\overline{u'v'}$ response to a positive $\bar{u}$ anomaly is the sum of a localized and positive IOR response and a broad and negative phase speed response (linear superposition nearly holds). Note that the broad phase speed response is not an artifact of the smoothing in the simple model of phase speed changes, because the response is also broad and negative when the smoothing is turned off (Fig. 5f). We offer an explanation for the broad phase speed response to local $\bar{u}$ changes in section 4e.

When we impose the $\bar{u}$ and β^* effects on the IOR separately (Figs. 5de), we see that the $\overline{u'v'}$ changes in the subtropics are almost entirely due to $\bar{u}$ while the changes poleward of 30° include contributions from both $\bar{u}$ and β^*. β^* has little effect on the $\overline{u'v'}$ in the subtropics because, as we show below, the movement of the critical level on the equatorward flank of the jet explains most of these $\overline{u'v'}$ anomalies. Poleward of 30°, we will see that the dynamics tend to be dominated by changes in the re-

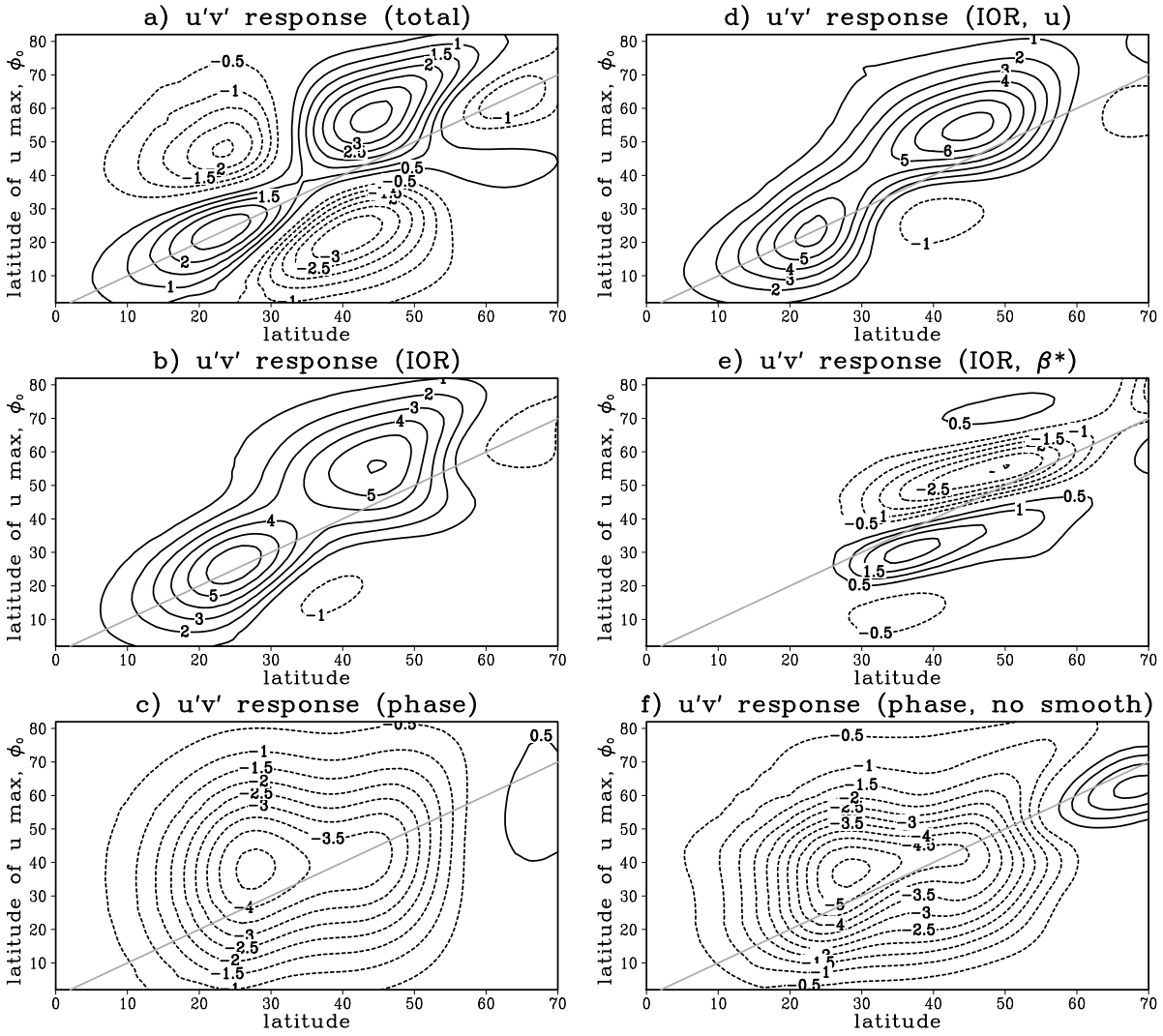

Figure 5: The RWC eddy momentum flux response (x-axis) to imposed $\bar{u}$ anomalies as a function of the latitude of the imposed $\bar{u}$ (y-axis). The eddy momentum flux is integrated over phase speed and wavenumber. The gray line is the line $y = x$. The units are m^2 s^{-2}. a) Total response. b) Response from changes in IOR. c) Response from changes in the phase speed of the wave activity source. d) Response from the effect of $\bar{u}$ alone on IOR. e) Response from the effect of β^* alone on IOR. f) As in (c) but for no smoothing of the background flow changes in the phase speed model.

flecting level as described in the Introduction. The effect of β^* is at a smaller "wave length" in ϕ_0 compared to $\bar{u}$ because the β^* anomalies are proportional to minus the second derivative of $\bar{u}$. When $\bar{u}$ is in phase with the latitude of the peak in the reflecting level of the dominant zonal wavenumbers ($\approx 52°$, see Lorenz (2014b)), $\bar{u}$ and β^* are both positive at 52° and therefore $\bar{u}$ increases wave reflection while β^* decreases wave reflection (see equation (1)). As a result, when ϕ_0 = 52°, the $\overline{u'v'}$ anomalies are positive for $\bar{u}$ (Fig. 5d) and negative for β^* (Fig. 5e). As the imposed $\bar{u}$ monopole shifts away from 52°, the value of β^* at 52° switches sign due to the change in curvature on the flanks of the Gaussian $\bar{u}$ anomaly. This explains the positive $\overline{u'v'}$ anomalies in Fig. 5e when ϕ_0 = 32° and 72°. More quantitative diagnostics of the effect of the reflecting level are included in the next section.

To summarize the effect of the eddies back onto the imposed $\bar{u}$, we project the eddy momentum forcing ($= \overline{\zeta' v'}$) onto the normalized $\bar{u}$ anomaly for each ϕ_0 (Fig. 6a). This quantifies the magnitude of the positive eddy feedback onto $\bar{u}$. The total eddy forcing is a positive feedback onto the wind anomalies when $\bar{u}$ is located at 28° or 52°. These latitudes are close to the centers of action of EOF1 (32° and 52°, Fig. 3b). Part of the dis-

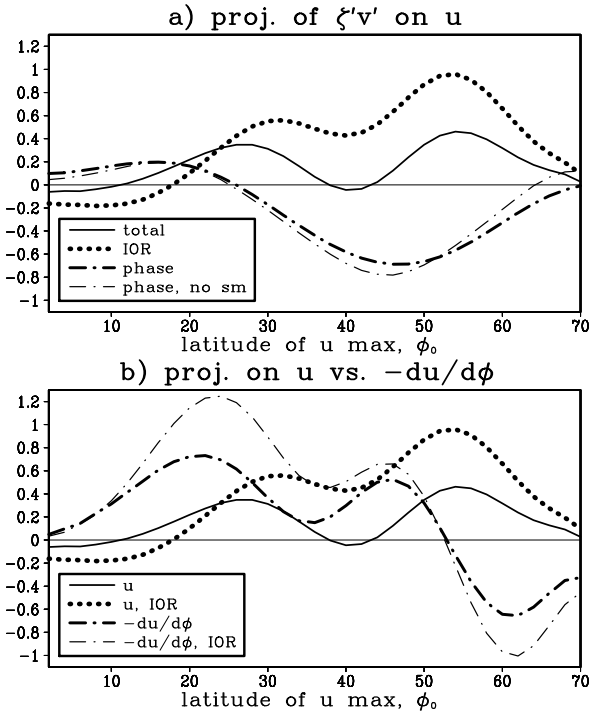

Figure 6: a) Projection of the RWC eddy vorticity flux response back onto the imposed Gaussian $\bar{u}$ anomaly as a function of the latitude of the imposed $\bar{u}$ (x-axis). The vorticity flux projections are separated into components: the total (thin solid), IOR induced (thick dotted), the phase speed induced (thick dash-dotted) and the phase speed induced with no smoothing in the phase speed model (thin dash-dotted). The units are m s^{-1} day^{-1}. b) The thin solid and thick dotted lines are the same as in (a). Also shown are the projections on the poleward propagation pattern ($= -d\bar{u}/d\phi$) for the total (thick dash-dotted) and IOR induced (thin dash-dotted) eddy vorticity flux.

crepancy in the location of the equatorward center of action can be resolved if we force the RWC model with narrower $\bar{u}$ more representative of the internal variability. As implied by Fig. 5, the structure of the positive feedback is derived from the IOR induced eddy fluxes (Fig. 6a). The latitudinal structure of the phase speed induced changes, on the other hand, changes relatively little with the latitude of $\bar{u}$. This insensitivity to $\bar{u}$ is not due to the smoothing present in the phase speed model because the structure of the phase speed feedback hardly changes when the smoothing is eliminated. Also, note the minimum in the positive feedback when $\bar{u}$ is collocated with the mean jet (= 42°). This is consistent with the fact that the eddy momentum fluxes do not reinforce variations associated with EOF2 (e.g. Lorenz and Hartmann (2001)). We have also performed experiments with imposed $\bar{u}$ dipoles (not shown). The most important difference between the monopole and dipole experiments is the magnitude of the phase speed effect. The phase speed effect is weak for the dipole because the contributions of positive $\bar{u}$ anomalies at one latitude are canceled by the contributions of negative $\bar{u}$ at another latitude.

Considerably more attention has been given to the positive feedback between EOF1 and the eddies than another form of coupling between $\bar{u}$ and $\overline{u'v'}$: the poleward (and equatorward) propagation of $\bar{u}$ anomalies (James and Dodd (1996); Feldstein (1998); Lee et al. (2007); Sparrow et al. (2009)). Therefore, in Fig. 6b, we compare the projection of $\overline{\zeta'v'}$ on the normalized $\bar{u}$ itself with the projection of $\overline{\zeta'v'}$ on the normalized $-d\bar{u}/d\phi$. For infinitesimal poleward shifts, $-d\bar{u}/d\phi$ describes the structure of the resulting anomalies and therefore the projection on $-d\bar{u}/d\phi$ quantifies the degree of poleward propagation (in the Northern Hemisphere).[1] When the imposed $\bar{u}$ monopoles are equatorward (poleward) of 52° the eddies act to shift the anomalies poleward (equatorward) (Fig. 6b). Hence, the latitude 52° is a center of attraction that anomalies at other latitudes tend to propagate toward. The latitude 52° is also the location of the poleward center of action of EOF1 and the peak of the reflecting level for the dominant waves (see below). Note there is a relative minima in the degree of poleward propagation near the location of the equatorward center of action of EOF1 (32°).

Because it is generally believed that a positive feedback between the leading EOF and eddies is responsible for the selection of the leading EOF (Lorenz and Hartmann (2001); Lorenz and Hartmann (2003)), the results in this section suggest that the RWC model can be used to understand the structure of the internal variability given that RWC model implies a positive feedback for anomalies in phase with EOF1 and no feedback (on $\bar{u}$ magnitude) for anomalies out of phase. We have already alluded to the key role of the latitude of the peak of the reflecting level on determining where $\bar{u}$ anomalies are stationary. We will discuss this further below after we come to a better understanding of the role of the subtropical critical level on the response to $\bar{u}$ anomalies equatorward of the mean jet. Also, note that the latitudinal profile of the wave activity source is fixed in these experiments, so in other words, there is no baroclinic feedback.

[1] For example, consider a small shift, δ, in the $\bar{u}$ profile: $\bar{u}(\phi - \delta)$. By a Taylor series: $\bar{u}(\phi - \delta) - \bar{u}(\phi) \approx -\delta d\bar{u}/d\phi$. Therefore the change in $\bar{u}$ for small shifts is proportional to $-d\bar{u}/d\phi$.

4. Dynamical Mechanisms

a. Critical level dynamics

In this section, we develop a mechanistic model to diagnose and separate the portion of the IOR $\overline{u'v'}$ response that is due to critical level dynamics on the equatorward flank of the jet. The key predictor of the $\overline{u'v'}$ changes in our model is the latitude of the critical level as a function of phase speed, $\phi_{CL}(c)$. Changes in $\phi_{CL}(c)$ determine the amount of expansion/contraction of the equatorward flank of the $\overline{u'v'}$ profile. Specifically, let $\xi(\phi, c, m) \equiv \overline{u'v'}\cos^2\phi$ (we multiply the momentum flux by $\cos^2\phi$ so that $\partial_\phi \xi$ is proportional to the divergence of the meridional wave activity flux) and $\Delta\phi_{CL}$ be the change in the critical level, then the change in ξ in the Northern Hemisphere is approximated by

$$\Delta\xi(\phi, c, m) = -\max\left(\frac{\partial \xi}{\partial \phi}, 0\right)\Delta\phi_{CL}, \qquad (5)$$

where we use the fact that the structure of an infinitesimal shift of a function is proportional to minus the first derivative of the function and we truncate the shift profile with the maximum function so that $\Delta\xi$ represents a "one-sided shift" (i.e. expansion/contraction) of only the equatorward flank, which is where the critical level induced dissipation is occurring. Note, though not documented in (5), $\Delta\xi$ is allowed to be non-zero only in the region of continuously positive $\partial\xi/\partial\phi$ in the vicinity of ϕ_{CL}: if a region of positive $\partial\xi/\partial\phi$ is separated from ϕ_{CL} by a region of negative $\partial\xi/\partial\phi$, then $\Delta\xi$ is always zero in that region.[2] A generalization of (5) to the Southern Hemisphere is straightforward.

To test the critical level diagnostic, we explore the imposed Gaussian profile experiments described in section 3 for the case where $\phi_0 = 26°$. A phase speed/latitude spectrum of the change in $\overline{u'v'}$ from IOR is shown in Fig. 7. The response is dominated by increased $\overline{u'v'}$ on the subtropical flank of the jet (Fig. 7a). The critical level model successfully captures the general response (Fig. 7b), which suggests that the response in the RWC model is dominated by an equatorward shift of the critical level in response to increased $\bar{u}$ on the subtropical flank of the jet. We find that there is some variability in the sensitivity of ξ to $\Delta\phi_{CL}$ depending on the zonal wavenumber and phase speed but that the predicted latitudinal structure is more reliable. Therefore, before we use the critical level model to diagnose the RWC experiments, we scale the prediction in (5) by the linear regression slope separately for each m and c.[3] The scaled critical level model improves some of the biases in the raw model (Fig. 7c). We should point out that the reason the response to this $\bar{u}$ perturbation seems so simple is that we have isolated the effect of IOR changes. In the GCM, a similar $\bar{u}$ perturbation would also change the phase speed of the waves,

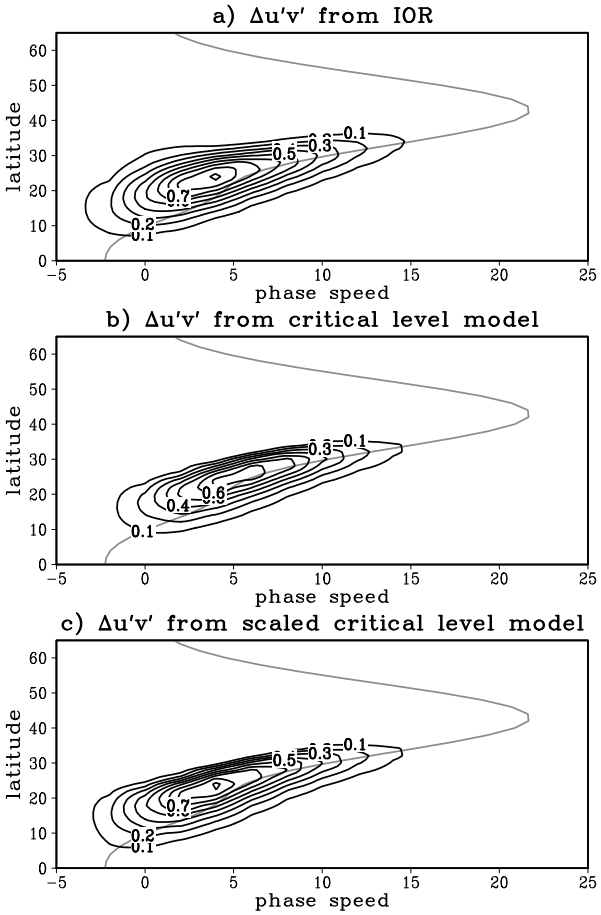

Figure 7: a) The change in the latitude/phase speed spectrum of the IOR induced RWC eddy momentum flux in response to a Gaussian $\bar{u}$ anomaly centered at 26°. The gray line is the critical level. The x-axis is angular phase speed in m s^{-1} at 45° (see section 2). b) As in (a) but for the mechanistic critical level model. c) As in (a) but for the scaled mechanistic critical level model (see text). The units are m s^{-1}.

[2] We find that the critical level model is more accurate when $\Delta\phi_{CL}$ is smoothed in phase before applying (5). For the results in this paper, we smooth $\Delta\phi_{CL}$ with the kernel: $\exp\left((c/w)^2\right)$, where w = 6.43 m s^{-1}.

[3] Let $y(\phi)$ be the latitudinal profile of $\overline{u'v'}$ for a single m and c from the RWC model and let $x(\phi)$ be the corresponding prediction from the simple critical level model (5). The scaled critical level model is given by $a_1 x(\phi)$ where $a_1 x + a_2$ is the linear least squares fit of y in terms of x.

resulting in a significantly more complicated pattern in the $\overline{u'v'}$ response.

b. Diagnosing the imposed zonal wind experiments

Here we use the scaled critical level model described above and the reflection diagnostic described in Lorenz (2014b) to diagnose the imposed $\bar{u}$ experiments in section 3. The diagnostics are applied to the $\overline{u'v'}$ response from IOR (Fig. 5b). First, we remove the $\overline{u'v'}$ portion related to the critical level on the equatorward flank. Next, we isolate the $\overline{u'v'}$ portion related to reflection on the poleward flank of the jet using the method in Lorenz (2014b).[4] Movements in the critical level dominate the $\overline{u'v'}$ response in the subtropics (Fig. 8a). In the mid-latitudes, the reflection diagnostic suggests that the reflectivity of the poleward flank accounts for about 80% of the $\overline{u'v'}$ response in the mid-latitudes (Fig. 8b). The residual is largest in the extratropics but is nevertheless less important than the other two terms (Fig. 8c). Physically, the residual might involve 1) the critical level on the poleward flank of the jet or 2) changes in the ability of waves to propagate *between* the critical and/or reflecting levels (i.e. changes involving meridional wave propagation in general rather than the changes directly involving either critical level absorption or reflection).

To quantify the feedbacks from critical and reflecting levels, we project the $\overline{\zeta'v'}$ anomalies on the imposed $\bar{u}$. The subtropical critical level is responsible for the positive feedback at the EOF1 center of action equatorward of the mean jet and for the weak negative feedback deep in the subtropics (Fig. 9a). The reflecting level, on the other hand, is responsible for much of the positive feedback at the EOF1 center of action poleward of the mean jet. Projecting the responses on $-d\bar{u}/d\phi$ (Fig. 9b), we see that the subtropical critical level is responsible for much of the poleward propagating anomalies in the subtropics as suggested by James and Dodd (1996) and Lee et al. (2007). When $\bar{u}$ is in phase with the time-mean jet (= 42°), on the other hand, reflection on the poleward flank acts to shift the anomaly poleward (Fig. 1f). The poleward shift for this in-phase $\bar{u}$ perturbation is due to the effect of the increases in zonal wind on the reflecting level on the poleward flank of the anomaly (1). The effect of β^* is nearly zero because the perturbation is not narrow enough for the negative β^* on the jet flanks to be in phase with the reflecting level maximum ($\approx 52°$) and thus does not act to increase the range of phase speeds encountering a reflecting level. We will consider effect of $\bar{u}$ scale in section 5. Note that most of the equatorward propagation poleward of 55° is not captured by the critical level or the reflecting level.

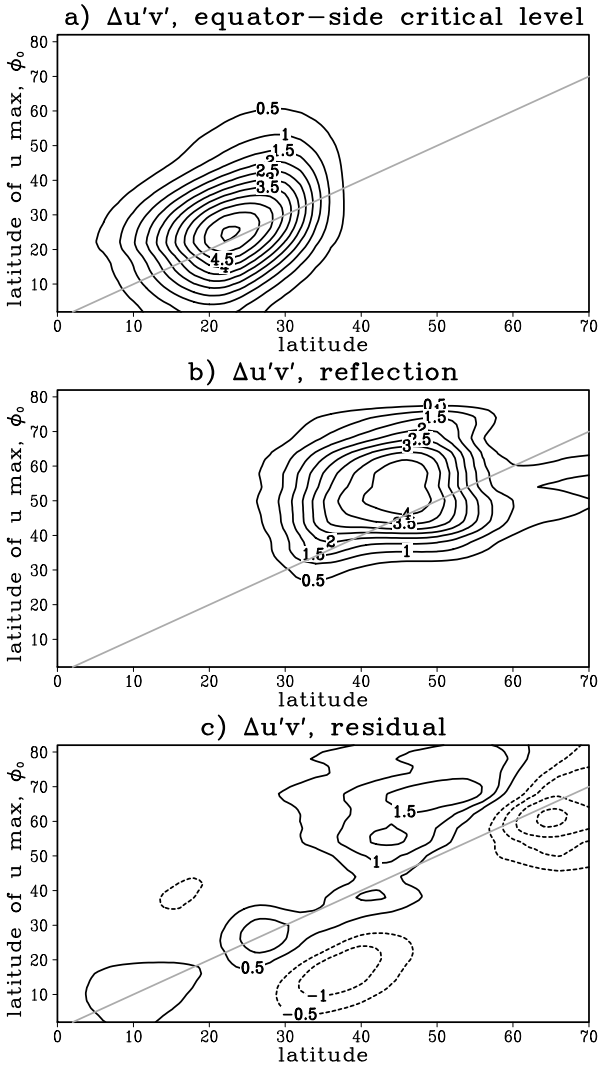

Figure 8: As in Fig. 5b but for the IOR induced RWC eddy momentum flux separated into components: a) latitudinal movement of the critical level on the equatorward flank of the jet, b) changes in the reflectivity of the poleward flank of the jet, and c) the residual (total IOR induced response minus (a) and (b)). The units are $m^2\ s^{-2}$.

c. Simplified reflecting level dynamics

In this section we develop a simplified model that simulates the effect of reflection on the $\overline{u'v'}$ response to

[4]The method involves explicitly calculating the reflectivity of index of refraction profiles using the inviscid wave equation ($\psi'' - l^2\psi = 0$, where l^2 is the index of refraction) in a manner analogous to the calculation of the reflectivity of quantum mechanical barriers with Schrödinger's equation.

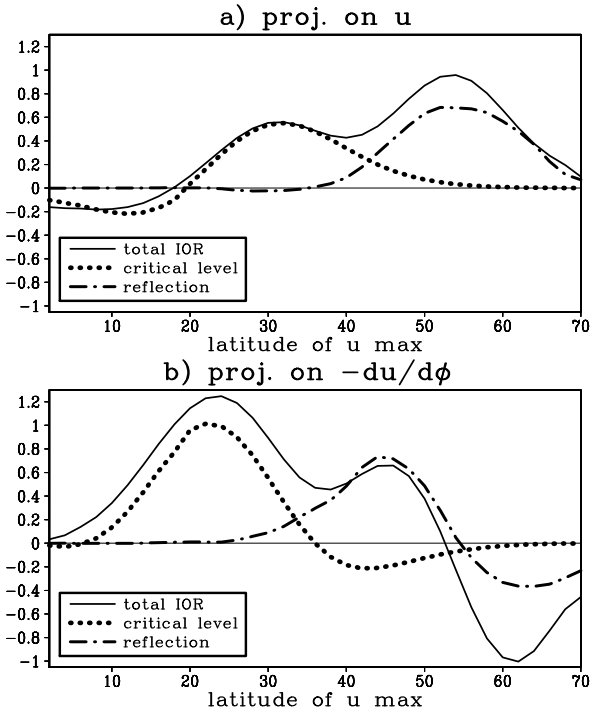

Figure 9: a) Projection of the RWC eddy vorticity flux response back onto the imposed Gaussian $\bar{u}$ anomaly as a function of the latitude of the imposed $\bar{u}$ (x-axis). The vorticity flux projections are separated into components: total IOR induced (thin solid), the portion from the critical level on the equatorward flank (thick dotted) and the portion from the reflectivity of the poleward flank of the jet (dash-dotted) (m s^{-1} day^{-1}). b) As in (a) but for the projection on the poleward propagation pattern ($= -d\bar{u}/d\phi$).

$\bar{u}$ anomalies. The model is based on more detailed study of the $\overline{u'v'}$ from reflection in response to imposed Gaussian wind anomalies discussed in the previous subsection. Consider the Gaussian wind anomaly profiles associated with ϕ_0 = 42°, 52° and 62° (Fig. 10a) and the corresponding $\overline{u'v'}$ profiles from reflection (Fig. 10b). Despite the large variation in the latitude of the imposed $\bar{u}$ anomalies, the $\overline{u'v'}$ anomalies are nearly stationary in latitude. The $\overline{u'v'}$ from reflection are nearly stationary because the location of the $\overline{u'v'}$ anomalies is fixed relative to the critical levels of the very limited range of waves with phase speeds near the phase speed of the peak in the reflecting level (see Fig. 1ef). In the nearly inviscid case, the $\overline{u'v'}$ anomalies from reflection simply extend from the poleward side critical level to the equatorward side critical level. With the strong diffusion in the RWC model (i.e. Lorenz (2014a)), however, most of the anomalies decay about 5 to 10° before reaching the subtropical critical level.

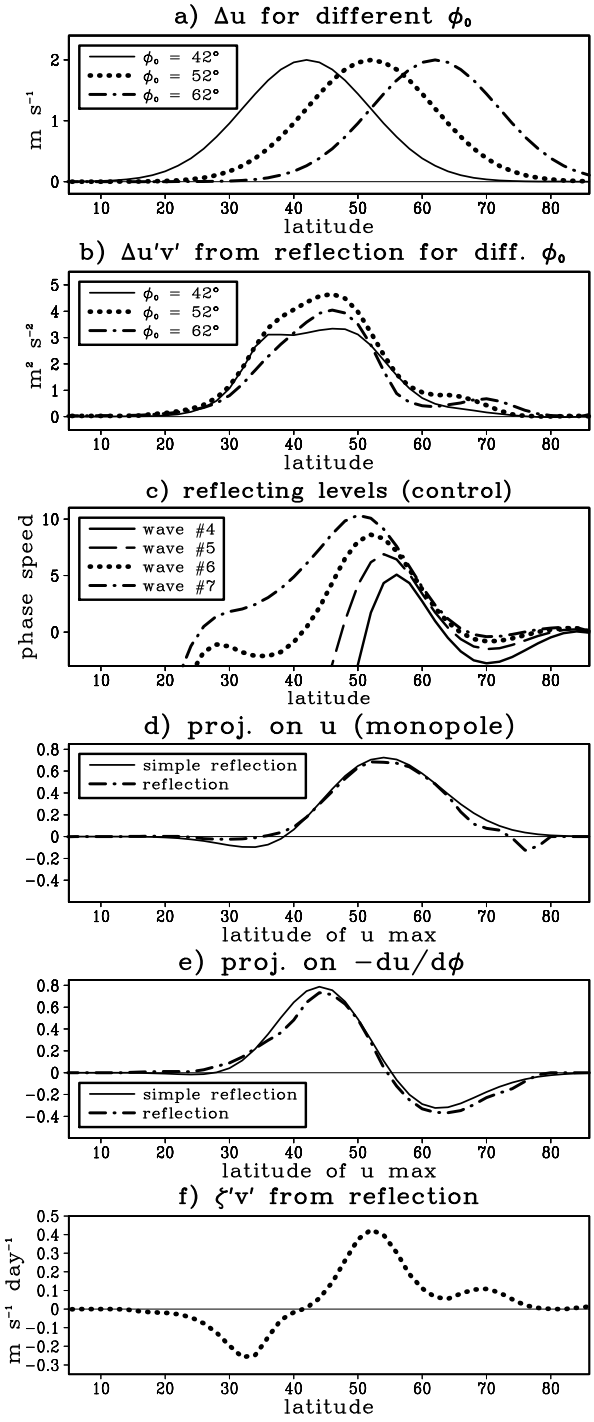

Figure 10: a) Imposed $\bar{u}$ anomalies of the form $2\exp\left(-((\phi-\phi_0)/14°)^2\right)$ m s^{-1}. b) The change in $\overline{u'v'}$ due to changes in reflection in the RWC model in response to the $\bar{u}$ anomalies in (a). c) The reflecting levels (1) for zonal wavenumbers 4, 5, 6 and 7 for the control run. d) The dash-dotted line is the same as in Fig. 9a. The thin solid line is the same projection but for the simplified reflecting level model. e) The dash-dotted line is the same as in Fig. 9b. The thin solid line is the same projection but for the simplified reflecting level model. f) The momentum flux convergence ($= \overline{\zeta' v'}$) associated with "reflection".

Another important characteristic of the $\overline{u'v'}$ anomalies from reflection is that they are solely determined by the changes in $\bar{u}$ and β^* at the latitude of the peak of the reflecting level (for small anomalies). Changes in the reflecting level at all other latitudes, on the other hand, only change the latitude of the reflection and not the range of phase speeds reflected. Because the reflecting level depends on the zonal wavenumber, some sensitivity to the latitude of $\bar{u}$ and β^* will be introduced. For the control run, however, the latitude of the peak in the reflecting level changes relatively little with wavenumber. For example, for the dominant zonal wavenumbers (4 - 8), the peak of the reflecting level only varies from 56° to 48°, respectively (Fig. 10c, only wavenumber 8 is not shown).

The above ideas suggest that the momentum fluxes from reflection can be parameterized as follows:

$$\overline{u'v'}_{\text{Refl}} = R(\phi)\Delta p(\phi_{\text{PRL}}), \tag{6}$$

where $R(\phi)$ is a fixed $\overline{u'v'}$ profile associated with reflection, ϕ_{PRL} is the latitude of the peak in the reflecting level and Δp is the change in the (angular) phase speed of the peak of the reflecting level:

$$\Delta p(\phi_{\text{PRL}}) = \left(\frac{\Delta \bar{u}(\phi_{\text{PRL}})}{a\cos\phi} - \frac{a\cos\phi \Delta\beta^*(\phi_{\text{PRL}})}{m^2} \right). \tag{7}$$

Note, (7) is simply derived from (1). Because a range of important wavenumbers are involved, we average Δp from 56° to 48° to account for the variability in ϕ_{PRL} for the dominant zonal wavenumbers (4 - 8). $R(\phi)$ is then simply set equal to the $\overline{u'v'}$ anomalies from reflection for the Gaussian profile with ϕ_0 = 52° divided by the average Δp defined above (we use $m = 7$). The parameterization obviously matches the reflection diagnosed from the RWC model when ϕ_0 = 52°, the question is whether the simple model captures the amplitude of the $\overline{u'v'}$ for other $\bar{u}$ anomalies. Therefore, we repeat the projection diagnostics in Fig. 9 but for the simple reflection model (Figs. 10de). Comparing the diagnosed reflection with the simple model, we see that the simple model does a very good job capturing the degree of positive feedback versus poleward propagation.

The momentum flux convergence ($= \overline{\zeta' v'}$) associated with $R(\phi)$ is shown in Fig. 10e. Because $\overline{\zeta' v'}$ is positive in the key latitude range (48 - 56°), this eddy forcing reinforces the changes in peak of reflecting level on poleward flank of the jet. Hence, there is a positive eddy feedback associated with $\bar{u}$ anomalies on the poleward flank. This positive feedback is also associated with opposite sign forcing on the equatorward flank of the jet, however, the resulting $\bar{u}$ anomaly is simply a result of momentum conservation and is not the trigger for the positive feedback. (We will discuss how critical level dynamics enters into the picture below.) The positive feedback also exists for negative $\bar{u}$ anomalies on the poleward flank and positive $\bar{u}$ anomalies on the equatorward flank. In this case, it is the negative $\bar{u}$ anomalies on the poleward flank that trigger the feedback via less reflection on the poleward flank of the jet. The above discussion suggests that dipole patterns associated with north/south shifts of the jet dominate when the peak of the reflecting level is on the poleward flank of the jet. We discuss the conditions for this situation in the conclusions.

d. Simplified critical level dynamics

In this section we further simplify the mechanistic critical level to help understand the relative effect of critical level dynamics on poleward propagation versus positive/negative feedback. Because the angular phase speed of linear waves is conserved in a steady and zonally symmetric background flow, the zonal wind used in the following analysis is scaled to make it proportional to the angular velocity:

$$u_A = u/\cos\phi. \tag{8}$$

Consider a zonal-mean zonal wind perturbation of small amplitude, $\delta\bar{u}_A$, and width, δw, to the flanks of a mean jet, $\bar{u}_A$. The change in the latitude of the critical level at the location of the perturbation is

$$\delta\phi_{CL} = -\frac{\delta\bar{u}_A}{\Lambda}, \tag{9}$$

where Λ is the mean shear, $d\bar{u}_A/d\phi$, at the critical level. As before, let $\xi(\phi, c, m)$ be the spectral density of $\overline{u'v'}$ multiplied by $\cos^2\phi$. The perturbation has width, δw, so the range of phase speeds affected by the perturbation is

$$\delta c = \Lambda \delta w. \tag{10}$$

Therefore, after substituting the expressions for $\delta\phi$ and δc, the perturbation momentum flux (over phase speed range, δc) from (5) is:

$$\Delta\xi(\phi, c, m)\delta c = \max\left(\frac{\partial\xi}{\partial\phi}, 0\right)\delta\bar{u}_A\delta w. \tag{11}$$

Like (5), this expression only holds in the Northern Hemisphere.[5] Note that the mean shear has dropped out of the expression because the effect of shear on the movement of the critical level is opposite the effect of shear on the range of phase speeds encountering an altered critical level. Suppose we let δw be the width of the grid spacing, then the total momentum flux change can be found by summing (11) over all c and m for each grid point while also noting that the correct $\delta\bar{u}_A$ is the $\delta\bar{u}_A$ at the critical level for waves with phase speed c. If the latitudinal separation between the critical level and the wave dissipation is small enough, however, the error from using the local $\delta\bar{u}_A$ instead of the $\delta\bar{u}_A$ at the critical level is small and one can simply integrate $\max\left(\frac{\partial\xi}{\partial\phi}, 0\right)$ over c and m beforehand, and then multiply by $\delta\bar{u}$ and δw. In this limit, the momentum flux response to small $\bar{u}$ anomalies is simply $\delta\bar{u}$ times a climatological profile of "wave dissipation", $D(\phi)$:

$$\delta\overline{u'v'}(\phi) = \frac{D(\phi)\delta\bar{u}_A(\phi)}{\cos^2\phi}, \tag{12}$$

where

$$D(\phi) = \sum_{c,m} \max\left(\frac{\partial\xi}{\partial\phi}, 0\right)\delta m\delta w, \tag{13}$$

δw is the grid spacing and the $\cos^2\phi$ factor comes from the fact that $\xi = \overline{u'v'}\cos^2\phi$. Note, there is no explicit δc in the sum in (13) because of (10). The climatological wave dissipation in the control run is centered at about 24° (Fig. 11a). We apply the simple critical level model given by (12) to the imposed $\bar{u}$ experiments in section 3. The model correctly predicts the transitions from negative feedback to poleward propagation to positive feedback as one moves from the equator to the pole, although the amplitude of the poleward propagation is too large (Figs. 11bc). When the $\bar{u}$ anomaly is in phase with D, then $\overline{u'v'}$ is also in phase with $\bar{u}$ (see (12)) and therefore the momentum flux *convergence* acts to shift the anomaly poleward. Critical level dynamics only begins to project positively on the $\bar{u}$ anomaly when the bulk of the climatological wave dissipation lies equatorward of the anomaly. In this case, the convergence of momentum flux that feedbacks positively on the anomaly is due to the convergence of the climatological D as represented by the first term in

[5]Multiply the right hand side by minus one for the Southern Hemisphere

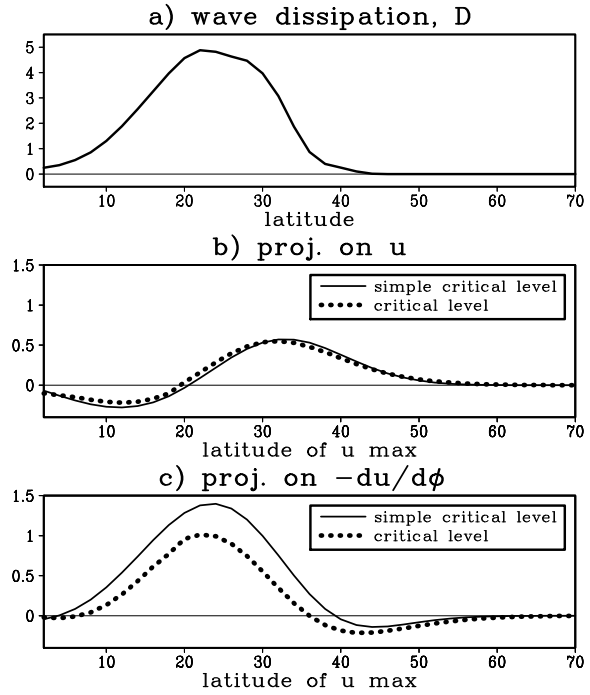

Figure 11: a) Climatological "wave dissipation" (= D, see text) in the control run. b) The thick dotted line is the same as in Fig. 9a. The thin solid line is the same projection but for the simplified critical level model involving only $\bar{u}$ and D. c) The thick dotted line is the same as in Fig. 9b. The thin solid line is the same projection but for the simplified critical level model involving only $\bar{u}$ and D.

the differentiation of (12) via the product rule:

$$-\frac{1}{\cos^2\phi}\frac{d\delta\overline{u'v'}\cos^2\phi}{d\phi} = -\frac{1}{\cos^2\phi}\frac{dD}{d\phi}\delta\bar{u}_A + \frac{1}{\cos^2\phi}\left(-\frac{d\delta\bar{u}_A}{d\phi}\right)D. \tag{14}$$

This first term is positive over the entire anomaly if the anomaly is entirely in the region of decreasing D. Likewise the second term represents different degrees of poleward shift depending on the amplitude of D (the small equatorward shift deep in the subtropics comes from the first term).

An analysis of the projection of $\zeta'v'$ on $\bar{u}$ hides the fact that $\bar{u}$ evolution under critical level dynamics follows a simple conservation equation with transport velocity D:

$$\frac{\partial\bar{u}}{\partial t} + \frac{\partial D\bar{u}}{\partial\phi} = 0, \tag{15}$$

where for simplicity we neglect the $\cos(\phi)$ factors and we drop the δ in front of $\bar{u}$. Because D is positive (negative) in the Northern (Southern) Hemisphere, critical level dynamics is always acting to shift the integrated $\bar{u}$ poleward toward the wave activity source. In addition, when there

is convergence (divergence) in D, critical level dynamics causes the anomaly to increase (decrease) in amplitude and decrease (increase) in meridional scale such that the integrated $\bar{u}$ remains constant.

For spherical geometry, the $\bar{u}\cos\phi$ evolution under critical level dynamics follows a simple conservation equation with transport velocity $D\cos^{-3}\phi$:

$$\frac{\partial \bar{u}\cos\phi}{\partial t} + \frac{1}{\cos\phi}\frac{\partial D\bar{u}_A}{\partial \phi} = 0 \tag{16}$$

$$\frac{\partial \bar{u}\cos\phi}{\partial t} + \frac{1}{\cos\phi}\frac{\partial\left(\cos\phi\left(D\cos^{-3}\phi\right)\bar{u}\cos\phi\right)}{\partial\phi} = 0.$$

e. Response to changes in phase speed

In this section we offer an explanation for the broad structure of the $\overline{u'v'}$ response to changes in wave activity source phase speed that is also relatively insensitive of the details of the imposed $\bar{u}$ anomalies.

Diagnostics in Lorenz (2014a) show that advection rather than β^* dominates the phase speed changes of the wave activity source. Hence the response to an imposed $\bar{u}$ anomaly is non-local in phase speed: both high and low phase speed waves change their phase speeds by about same amount. Consider the response to an increase in $\bar{u}$. If all waves increase phase speeds by the same amount, then, after a Galilean transform, the response is like that of a decrease in winds everywhere while keeping phase constant. This implies both critical and reflecting level dynamics come into play but in the opposite direction from the effect of $\bar{u}$ increases on IOR. The combination of the subtropical critical level $\overline{u'v'}$ and the mid-latitude reflecting level $\overline{u'v'}$ gives rise to the broad phase speed response seen above. The results in Figs. 5 and 6 and the response to poleward shifted jets (Lorenz (2014b)) suggest that the broad response of $\overline{u'v'}$ to changes in phase speed appears even when $\bar{u}$ is localized in latitude. We believe the response is broad in this case because the meridional propagation of wave activity implies that localized wave source changes nevertheless impact all latitudes accessible via wave propagation. Because the wave source spectrum is broad in phase speed (Fig. 4a), this means that a wide range of latitudes are accessible to waves and therefore the $\overline{u'v'}$ response is broad.

If the effect of phase speed on $\overline{u'v'}$ is opposite the effect of IOR, why is the IOR effect larger in the experiments shown above and in the response to external forcing in Lorenz (2014b)? The dominance of IOR depends on the scale of the imposed $\bar{u}$. For example, when we impose a broad constant angular velocity perturbation in the RWC model ($\bar{u} = 2\cos\phi$ m s^{-1}) the IOR and phase speed effects nearly cancel (not shown). When the $\bar{u}$ scale is smaller than the scale of the wave activity source region, however, the IOR response is larger. This effect is easiest to understand when considering the reflecting level. For sake of discussion, we will ignore the effect of β^* anomalies. Therefore, to increase the peak of reflecting level by 1 m s^{-1}, we only need to increase $\bar{u}$ by 1 m s^{-1} at the location of the peak in the reflecting level. This *local* change in the reflecting level affects *all* waves propagating toward the poleward flank of the jet. To increase the phase speed of *all* waves propagating poleward toward the reflecting or critical level by 1 m s^{-1}, on the other hand, we need to increase $\bar{u}$ across *all* source latitudes by 1 m s^{-1}. Therefore, a well placed local $\bar{u}$ anomaly will have a much bigger impact on the waves through the IOR than through the phase speeds of the wave sources. For local $\bar{u}$ anomalies on the subtropical flank of the jet, the local critical level moves according to the *local* $\bar{u}$ while the net phase speed change of the waves impinging on the critical level changes by a significantly smaller amount because some of these waves have source latitudes far removed from the local $\bar{u}$ anomaly. In summary, IOR dominates because the *net* phase speed change is an integrator of $\bar{u}$ across the entire width of the wave source region while IOR can respond strongly to well-positioned *local* $\bar{u}$ anomalies.

The above discussion suggests that phase speed effects are most important for $\bar{u}$ anomalies at the latitude of the mean jet. Indeed the effect of phase speed cancels the positive IOR feedback when the imposed $\bar{u}$ is at 42° (Fig. 6a). However, this is also a region where the IOR leads to strong poleward propagation via changes in the reflecting level on the poleward flank (Fig. 6b). If, on the other hand, the $\bar{u}$ anomaly is narrow enough to not disturb peak of reflecting level then it is also too narrow to be maintained: the eddies will immediately act to broaden anomaly and will eventually shift the anomaly poleward via reflecting level dynamics (see next section).

In Lorenz (2014a), we noted that changes in wave scale (Kidston et al. (2011)) and/or β^* can potentially change the phase speed of the wave activity sources relative to $\bar{u}$ and this may help stronger jets shift poleward. While the wave scale changes are in fact weak (Lorenz (2014a)), the changes in β^* associated with a stronger jet act to reduce the phase speed of the waves in the jet core.

The sense of this change is to increase the range of phase speeds that reflect leading to a poleward shift. To quantify this effect we redo the reduced friction RWC coupled experiments in section 6 of Lorenz (2014a) but with only advection affecting the wave source phase speeds. In this experiment there is essentially no change in the magnitude of the response. This suggests that for the type of $\bar{u}$ perturbations considered here, the effect of β^* and wave scale on $\overline{u'v'}$ via changes in the relative phase speed are negligible compared to the mechanisms discussed above.

5. Response as a function of zonal wind width

In this section we briefly discuss the response of the RWC model to $\bar{u}$ anomalies of different meridional scales that are in phase with the time mean jet. In section 4, we noted that for our particular (positive) $\bar{u}$ anomalies, it is $\bar{u}$ rather than β^* that causes the peak of reflecting level to increase when $\bar{u}$ is in phase with the mean jet. In this case, the negative β^* anomaly (associated with the positive curvature of $\bar{u}$) is too far poleward relative to the peak in the reflecting level for the dominant zonal wavenumbers. This implies, however, that smaller scale anomalies will "excite" the reflecting level via changes in β^*. While this is indeed the case, the eddy feedback for these small scale anomalies is much better described as a negative feedback acting to broaden the anomaly. In other words, while there are momentum fluxes poleward of the anomaly acting to shift the anomaly poleward there are also similar magnitude momentum fluxes equatorward of the anomaly acting to shift the anomaly equatorward. For example, consider the response of the critical and reflecting levels to an imposed $\bar{u}$ anomaly of the form $1.5 \exp\left(-((\phi-\phi_0)/w_0)^2\right)$ m s^{-1}, where $\phi_0 = 45°$ and $w_0 = 5°$ (Fig. 12a). In this case, the increase in the reflecting level peak is due to the decreases in β^* on the flanks of the narrow $\bar{u}$ anomaly. Note that in addition to the increase in the main peak of the reflecting level, there is an additional secondary peak that develops at about 35°. The $\overline{u'v'}$ anomalies associated with this wind anomaly show the typical positive anomalies in the vicinity of the primary peak in the reflecting level, however, they also show negative anomalies in the vicinity of the secondary reflecting level peak (Fig. 12b). It appears that the secondary reflecting level peak blocks the equatorward propagation of wave activity leading to the negative $\overline{u'v'}$ anomalies. Taken together, the positive and negative $\overline{u'v'}$ anomalies are best described as a feedback

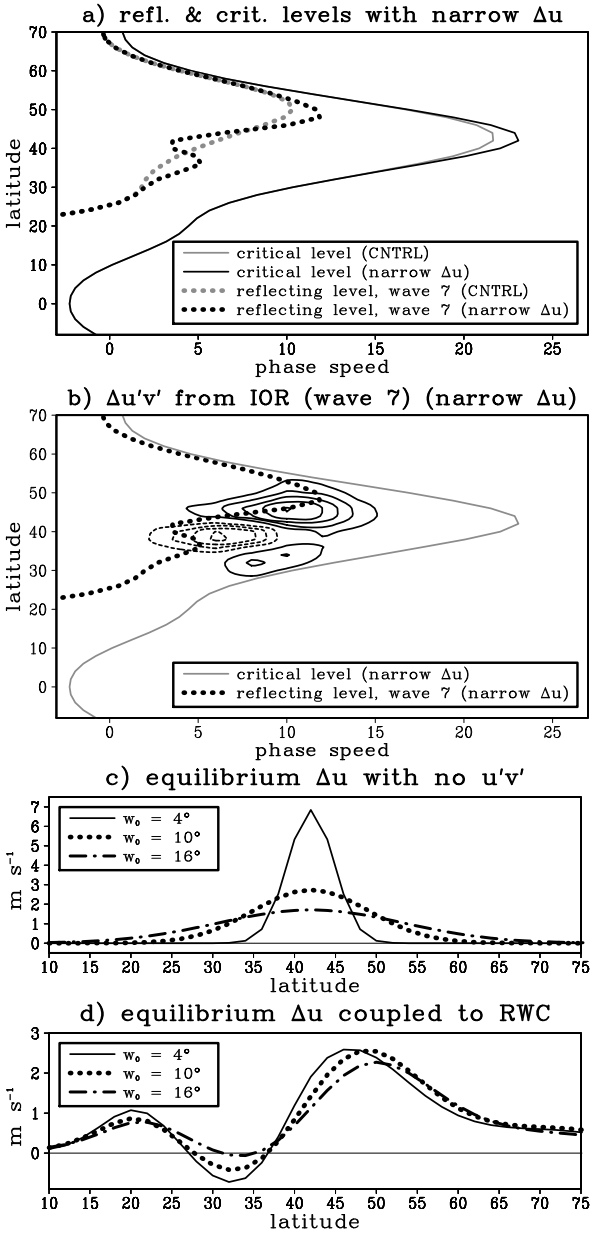

Figure 12: a) The critical (thin, solid) and reflecting (thick ,dotted) levels for the control (gray) and for the control plus a narrow $\bar{u}$ anomaly (black). The reflecting levels are for wavenumber 7. b) The change in the latitude/phase speed spectrum of $\overline{u'v'}$ for zonal wavenumber 7. Contour interval = 0.03 m s^{-1}. Also shown are the critical (thin, solid, gray) and reflecting (thick, dotted, black) levels for the narrow $\bar{u}$ anomaly case in (a). c) The long term response of the simple barotropic $\bar{u}$ model (4) with no eddies ($h = 0$) in response to forcing of various widths and amplitudes. d) As in (c) but when the eddy $\overline{\zeta'v'}$ from the RWC model is coupled to the simple barotropic $\bar{u}$ model.

acting to broaden the imposed $\bar{u}$ anomaly.

While the initial eddy fluxes and $\bar{u}$ tendency are strongly dependent on the scale of the imposed Gaussian anomaly (w_0), the long-term response when $\bar{u}$ and $\overline{u'v'}$ are coupled is not. For example, consider three coupled RWC experiments (see section 2 and Lorenz (2014a)) with different scale external $\bar{u}$ forcing ($w_0 = 4$, 10 and 16°) applied at the latitude of the time mean jet. (The forcing scale and amplitude are inversely related in these experiments so that the latitudinally integrated $\bar{u}$ force is constant.) The equilibrium $\bar{u}$ with no eddies results in dramatically different $\bar{u}$ anomaly profiles (Fig. 11c). When the RWC fluxes feedback on the $\bar{u}$ anomalies, however, the responses show a remarkably similar poleward shift pattern (Fig. 11d). Apparently negative feedbacks associated with $\bar{u}$ scale actively select the preferred width of the resulting $\bar{u}$ anomalies. In the next section, we explore the long-term response of the coupled RWC and $\bar{u}$ system in more detail.

6. Coupled System

Above we found that when imposed $\bar{u}$ anomalies are out of phase with EOF1, the eddies act to shift the anomalies either poleward or equatorward toward the EOF1 structure (Figs. 6b). This suggests that the long-term response of the coupled RWC system will project on EOF1 regardless of the structure of the forcing. We find this is indeed the case. In Fig. 13, we show the equilibrium $\bar{u}$ and $\overline{u'v'}$ profile as a function of the latitude, ϕ_0, of imposed mechanical forcing with a Gaussian profile.[6] As in Fig. 5a, $\phi_0 = 38°$, which is between the equatorward center of action of EOF1 and the time mean jet, is a key latitude separating the type of response. In this case, forcing equatorward (poleward) of 38° leads to the negative (positive) phase of EOF1. These results are likely relevant for the response of the jet to El Niño versus global warming: in contrast to global warming which acts to strengthen the jet, El Niño is associated with increased temperature gradients deeper in the subtropics. The associated direct $\bar{u}$ response is therefore equatorward of the time mean jet and is therefore associated with an equatorward shift of the jet (Sun et al. (2013)).

The $\overline{u'v'}$ response is interesting in that the mid-latitude $\overline{u'v'}$ dominates over the subtropical $\overline{u'v'}$ even in the case of forcing deep in the tropics (Fig. 13b). In the tropical forcing case, the $\overline{u'v'}$ decreases in the mid-latitudes are related to the changes in the reflecting level caused by the $\bar{u}$ decreases at poleward center of action of EOF1. How is the reflecting level altered in the first place? Based on Fig. 5, the adjustment appears to proceed as follows: 1) critical level dynamics act to shift the imposed $\bar{u}$ poleward resulting in positive anomalies at the equatorward center of action of EOF1. 2) At the same time, these anomalies increase the phase speeds of the waves, leading to decreased reflection and negative $\bar{u}$ on the poleward flank of the jet. 3) The negative $\bar{u}$ then excites the positive feedback between $\bar{u}$ and the reflecting level on the poleward flank. This mechanism is consistent with the equilibrium response in a new series of experiments where the source phase speeds remain constant (13cd). When the latitude of the forcing, ϕ_0, is less than 32°, the $\bar{u}$ and $\overline{u'v'}$ responses are mostly restricted equatorward of the time mean jet (42°). Also note that the $\bar{u}$ response is smaller for the case where phase speed is fixed. This is consistent with Fig. 6a, which shows that phase speed changes are associated with a positive feedback for anomalies equatorward of 25° (such anomalies happen to be in phase with the fixed location of subtropical drag associated with any increase in phase speed). When the latitude of the forcing is in the extratropics, on the other hand, the fixed phase speed experiments show a much stronger response because the negative phase speed feedback is no longer present.

In the extratropical forcing case, the dominance of the mid-latitude $\overline{u'v'}$ in the long-term response (Fig. 13b) appears to be related to subtle wind changes present in the subtropics. The mid-latitude $\overline{u'v'}$ also eventually dominates in the RWC response to EOF1 wind anomalies. For example, while the RWC model response to EOF1 anomalies is initially a $\overline{u'v'}$ dipole, this soon adjusts to a $\overline{u'v'}$ monopole (Fig. 14a). This monopole structure is like the monopole structure in lagged regressions of $\overline{u'v'}$ on EOF1 in the full GCM (when EOF1 leads $\overline{u'v'}$) (not shown). The initial dipole structure is much like the $\overline{u'v'}$ dipoles in the prescribed $\bar{u}$ experiments (Fig. 5a). A dipolar $\overline{u'v'}$ forces a tripolar $\bar{u}$ and this is evident in Fig. 14b with the growth of $\bar{u}$ anomalies in the subtropics and the slight poleward shift of the anomaly at 32°. The subtropical winds do not need to adjust much, however, before the subtropical $\overline{u'v'}$ anomalies disappear. By turning off the phase speed effect, we have verified that the feedback responsible for this adjustment does not involve changes in phase speed (because of the integrating

[6] The precise form of the forcing, F_z, in (4) is $F_z = 1.14 \cdot 2/\tau \exp\left(-((\phi - \phi_0)/12°)^2\right)$.

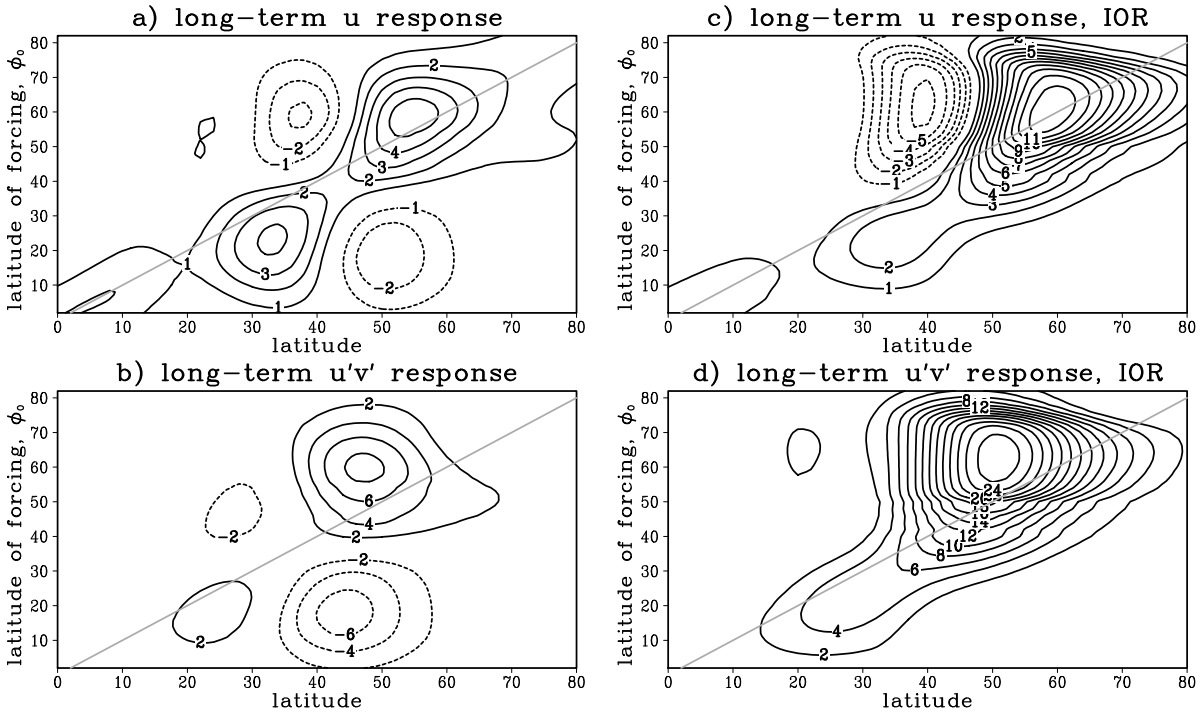

Figure 13: a) Equilibrium $\bar{u}$ response (x-axis) as a function of the latitude of imposed, Gaussian mechanical forcing (y-axis) in the coupled RWC model (m s^{-1}). The gray line is the line $y = x$. b) Same as (a) but for the eddy momentum flux (m^2 s^{-2}). c) Same as (a) but for the coupled RWC model with no changes in the phase speed of the wave activity source. d) Same as (c) but for the eddy momentum flux.

effect of the phase speed induced $\overline{u'v'}$, the role of phase speeds changes for $\bar{u}$ dipoles is very weak). We believe that the presence of an adjustment in the first place is due to RWC biases and that the RWC model is simply adjusting to its own version of the most persistent mode. The adjusted $\bar{u}$ pattern is not very different from the GCM EOF1 (Fig. 14c), but it has a large effect on the structure of $\overline{u'v'}$.

To understand the dominance of the mid-latitude $\overline{u'v'}$ in the long-term response, we run the same EOF1 initial value experiment with the simple reflecting and critical level models described in sections 4c and 4d taking the place of the RWC model in (4).[7] The evolution of $\overline{u'v'}$ and $\bar{u}$ for the simple model is shown in Figs. 15ab. The simple model reproduces the slight poleward shift and the gradual disappearance of the negative $\overline{u'v'}$ in the subtropics and the slight poleward shift of the equatorward center of action of $\bar{u}$. In this case, however, the negative $\bar{u}$ anomalies are too narrow and too far poleward compared to the coupled RWC model and the positive $\bar{u}$ anomalies deeper in the tropics are too weak to be seen with the current contour interval. To help understand the dominance of the mid-latitude $\overline{u'v'}$, we show the $\overline{u'v'}$ at time 30 days from the critical and reflecting level models as well as the total $\overline{u'v'}$ (Fig. 15c). The total $\overline{u'v'}$ has a positive monopole structure that is the combination of a broad, positive reflecting contribution and a narrower, negative critical level contribution. Like the prescribed $\bar{u}$ experiments in Fig. 8, the critical level contribution is non-negligible, however, it is smaller in absolute value than the positive reflecting contribution. Given the strong tendency for the $\overline{u'v'}$ associated with critical level dynamics to shift poleward (see section 4d), it appears that the critical level contribution simply propagates poleward until it is "hidden" by the stationary reflecting contribution (see

[7]Because the simple critical level model over-estimates the poleward propagation (Fig. 11c), we scale the simple critical level model by a factor of 0.73. Similarly, the reflection diagnostic underestmiates the momentum fluxes across the jet (Fig. 8b). Therefore we scale the simple reflecting model by a factor of 1.20. These constants are determined by a least squares fit of the simple models to Fig. 5b. Also, there is no change in the phase speeds of the wave sources in this experiment because the effect of phase speeds is weak for nearly symmetric dipoles. It is straightforward to add a reasonable the phase speed contribution, however, by simply adding or subtracting a constant from the input angular velocity ($\bar{u}/\cos\phi$) before applying the simple reflecting and critical level models. This constant is equal to the "average" angular phase speed change of the wave sources.

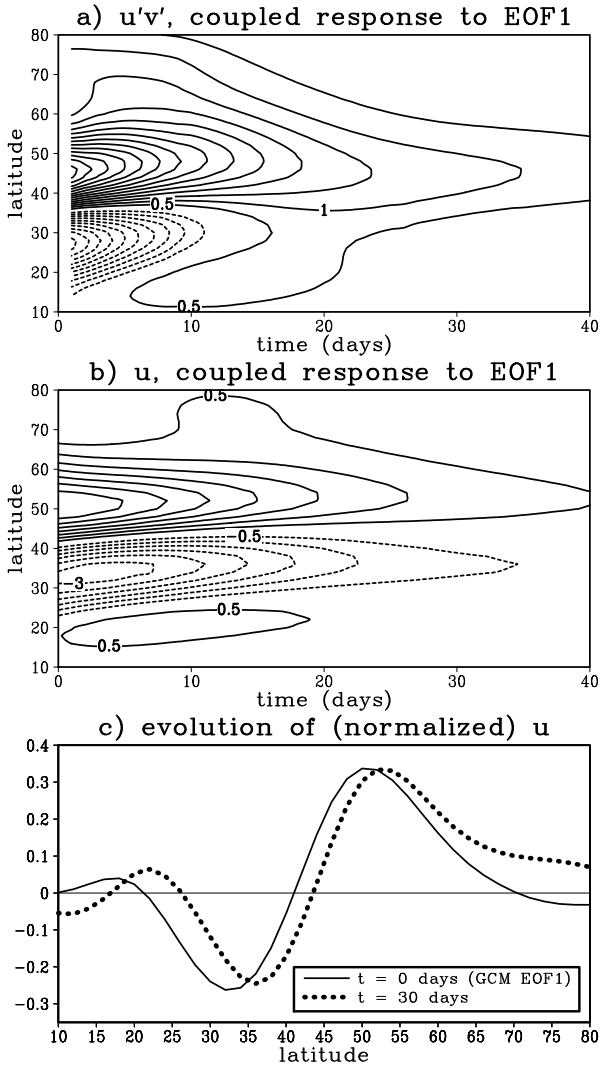

Figure 14: a) Evolution of eddy momentum flux anomalies in the unforced coupled RWC model with a positive EOF1 initial condition minus the evolution for a negative EOF1 initial condition (m^2 s^{-2}). The initial EOF1 pattern is from the GCM. b) As in (a) but for $\bar{u}$ (m s^{-1}). c) The normalized $\bar{u}$ profile for the initial condition (thin solid) and for time = 30 days (thick dotted).

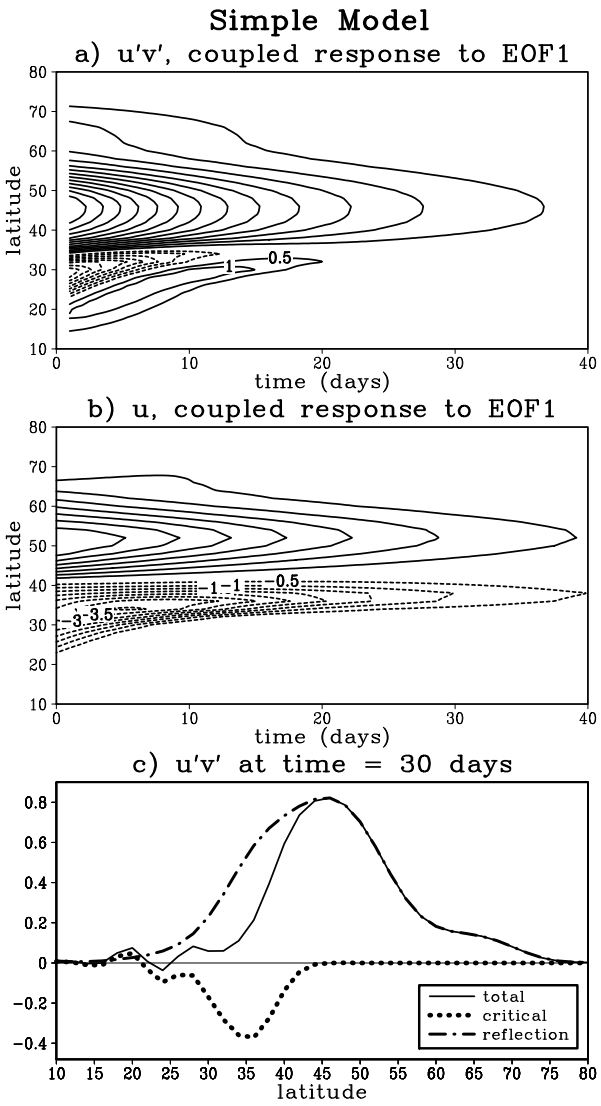

Figure 15: a) As in Fig. 14a but for the simple reflection and critical level models. b) As in Fig. 14b but for the simple reflecting and critical level models. c) The momentum flux at time = 30 days from the simple reflecting (dash-dotted) and critical (dotted) level models. The sum of the reflecting and critical level contributions is also shown (solid) (m^2 s^{-2}).

section 4c for an explanation of why the reflection contribution is stationary in latitude). Such poleward propagation is evident in the subtropics in both Fig. 14 and Fig. 15. Therefore the dominance of the mid-latitude $\overline{u'v'}$ is a consequence of the fact that the subtropical $\overline{u'v'}$ are inherently poleward propagating and are therefore transient. The mid-latitude $\overline{u'v'}$, on the other hand, reinforce and are consistent with a stationary $\bar{u}$ anomaly at the latitude of the peak in the reflecting level on the poleward flank of the jet.

7. Discussion and Conclusions

This is part III of a series of papers using Rossby Wave Chromatography (RWC) (Held and Phillips (1987)) to understand the variability and response to external forcing of an idealized GCM. By RWC, we mean that we calculate the space-time (i.e. phase speed-latitude-wavenumber) structure of the upper tropospheric eddy momentum fluxes given the background zonal-mean flow and the space-time structure of the baroclinic wave activity source (convergence of vertical EP flux (Edmon et al.

(1980)) in the upper troposphere).

The focus in this paper is on documenting and understanding the coupling between $\bar{u}$ anomalies and the eddy fluxes predicted by RWC. This study is limited to the case of $\bar{u}$ anomalies that are essentially barotropic in the sense that 1) the $\bar{u}$ tendency is well approximated by the sum of the eddy momentum flux convergence and a simple Rayleigh damping term acting on $\bar{u}$ and 2) the wave activity source integrated over phase speed is constant. We also consider changes in the phase speeds of the wave activity sources. These assumptions will be relaxed in future work.

We run a series of RWC experiments with imposed $\bar{u}$ monopoles at different latitudes. We find that the eddies reinforce the imposed $\bar{u}$ when it is collocated with the centers of action of EOF1 of the GCM. Reflecting level dynamics (Kidston and Vallis (2012); Lorenz (2014b)) are essential for the positive feedback when $\bar{u}$ is poleward of the jet and critical level dynamics (that are independent of phase speed changes) are essential for the positive feedback when $\bar{u}$ is equatorward of the jet. When the imposed $\bar{u}$ is out of phase with EOF1, the eddies tend to shift the imposed $\bar{u}$ poleward (equatorward) for anomalies that are equatorward (poleward) of the poleward center of action of EOF1. For localized $\bar{u}$ anomalies, critical level dynamics is most important for the poleward shift in the subtropics while reflecting level dynamics is most important for the poleward shift in the mid-latitudes. We provide simple models of critical and reflecting level dynamics that explain the degree of poleward propagation versus positive feedback in this series of experiments.

Looking at the imposed $\bar{u}$ experiments as a whole, we find that all of the dramatic changes in the structure of the momentum fluxes that occur as one changes the $\bar{u}$ latitude are due to changes in Index Of Refraction (IOR). The changes in momentum fluxes due to changes in wave source phase speed, on the other hand, always have the same broad monopole structure that gradually changes in amplitude as the $\bar{u}$ latitude changes. We believe this $\overline{u'v'}$ response is broad because the meridional propagation of wave activity implies that localized wave source changes nevertheless impact all latitudes accessible via wave propagation. Because the wave source spectrum is broad in phase speed (Fig. 4a), this means that a wide range of latitudes are accessible to waves and therefore the $\overline{u'v'}$ response is broad. Similarly, we also find that for local $\bar{u}$ anomalies, IOR effects on $\overline{u'v'}$ tend to dominate over phase speed because the *net* phase speed change is an integrator of $\bar{u}$ across the entire width of the wave source region while IOR is not.

In the imposed $\bar{u}$ experiments the $\overline{u'v'}$ anomalies are focused in two separate latitude bands: one in the subtropics and one in the mid-latitudes. When $\bar{u}$ and $\overline{u'v'}$ are coupled, however, the $\overline{u'v'}$ tends to adjust so that the mid-latitude $\overline{u'v'}$ dominates over the subtropical $\overline{u'v'}$. The monopole structure of the adjusted $\overline{u'v'}$ is consistent with the response of $\overline{u'v'}$ to EOF1 in the GCM (as diagnosed by lagged regressions). The dominance of the mid-latitude $\overline{u'v'}$ is a consequence of the fact that the subtropical $\overline{u'v'}$ (associated with critical level dynamics) are inherently poleward propagating and are therefore transient while the mid-latitude $\overline{u'v'}$, on the other hand, are consistent with a stationary $\bar{u}$ pattern.

Given that the $\overline{u'v'}$ adjusts so that the mid-latitude fluxes across the jet axis dominate, the key for understanding the structure of the leading EOF1 appears to be the location of the peak of the reflecting level on the poleward flank of the jet. While the peak in the reflecting level is wavenumber dependent, in our GCM the peak of the reflecting level only varies from 56° to 48° for the dominant wavenumbers 4 - 8. This explains why the structure of the reflecting level induced $\overline{u'v'}$ is insensitive to the precise location of the $\bar{u}$ anomalies. As long as $\bar{u}$ "excites" the reflecting level, there will be strong momentum flux divergence/convergence near the "average" reflecting level peak ($\approx 52°$, Figs. 10cf). Therefore patterns of variability that are in phase with the reflecting level peak dominate over other patterns (as long as the meridional scale of the anomaly is large enough that $\bar{u}$ dominates over β^* in (1)). The above ideas focus on the poleward center of action of EOF1 as the trigger for the positive eddy feedback. Although the location of the equatorward center of action of EOF1 is associated with reinforcing $\overline{u'v'}$ anomalies in the subtropics for generic, prescribed $\bar{u}$ anomalies (Fig. 6), the coupled $\bar{u}$ adjusts so that these subtropical $\overline{u'v'}$ anomalies disappear. This suggests that critical level dynamics associated with anomalies at the equatorward center of action of EOF1 play a secondary role in the positive feedback.

The above ideas suggest that latitudinal shifts of the jet dominate the variability only if the peak of the reflecting level is on the poleward flank of the jet. What conditions ensure that the reflecting level is on the poleward flank of the jet? The reflecting level is on the poleward flank provided the jet is narrow enough that variations in β^*, which is large in the jet and small on the flanks, are

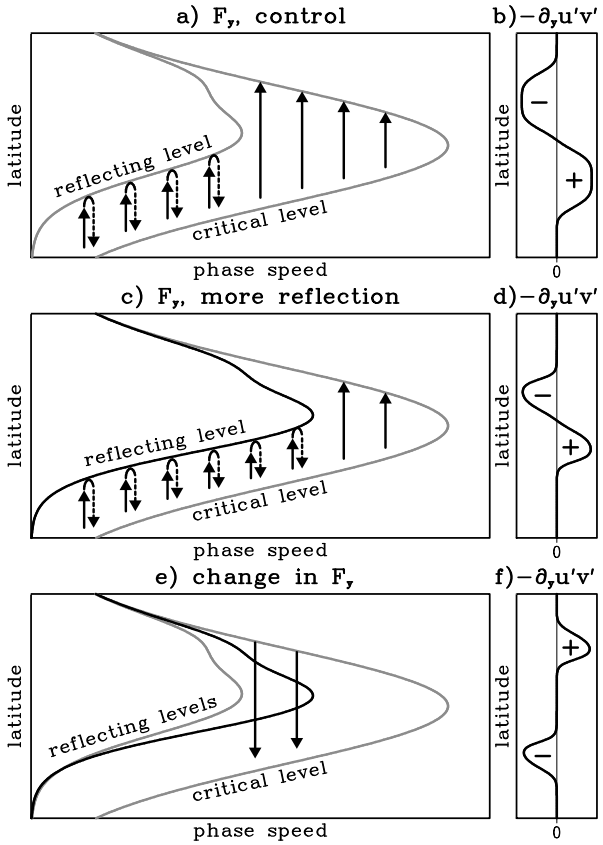

Figure 16: Reflection schematic: as in Fig. 1 but for the case where the peak of the reflecting level is close to the latitude of the climatological jet. The momentum flux convergence patterns are essentially the same as in Fig. 1 but now these eddy forcing patterns are optimally "excited" when $\bar{u}$ anomalies are nearly in phase with the time-mean jet rather than on the poleward flank. The eddies now shift the "optimal" $\bar{u}$ anomalies poleward rather than reinforcing them (see text).

large enough compared to $\bar{u}$ in (1). If β^* gets too small on the poleward flank, however, then the peak of the reflecting level could potentially extend to phase speeds beyond where there are significant wave activity sources, leading to a decrease in the positive feedback. This provides a slightly different explanation of the decrease in the positive feedback with latitude (Barnes et al. (2010); Barnes and Hartmann (2011)) in that it is the reflecting level itself that is responsible for the positive feedback.

If, on the other hand, β^* is not "large" compared to $\bar{u}$ (for example, the jet is broad), then the peak of the reflecting level approaches the latitude of the mean jet and the situation is like that depicted in Fig. 16. In this case, the momentum flux convergence associated with changes in the peak of the reflecting level remains on the poleward flank, however, the peak of the reflecting level now responds most strongly to $\bar{u}$ anomalies that are nearly in phase with the jet. This suggests that there is no dominant EOF in this case and that instead the dominant form of $\bar{u}$ variability is poleward propagating anomalies. This is consistent with the results of Lee et al. (2007) who found that poleward propagating anomalies dominate when mean potential vorticity gradients are weak. The peak of the reflecting level might also be displaced when a strong "subtropical jet" is present on the equatorward flank of the jet. Indeed, in Barnes and Hartmann (2011) the relative minimum in aK^* (= $\sqrt{l^2+m^2}$ in our notation) approaches the latitude of the mid-latitude jet as the subtropical jet becomes more important and the positive eddy feedback decreases in strength (their Fig. 12).[8] Barnes and Hartmann (2011) also show interesting jet states where the distribution of jet latitude is bimodal (their Fig. 14). In these cases, the dominant flank for reflection (as diagnosed by their aK^* profiles) actually changes from poleward flank of the jet to the equatorward flank of the jet depending on the state of the jet! The bimodality is likely associated with a complete change in dominant direction of wave activity propagation (for a certain class of waves). In the future, we plan to diagnose a large number of GCM runs with different means states to understand the effect of critical and reflecting level configuration on the character of the internal variability.

Finally, the results of this paper suggest that barotropic dynamics can account for the spatial structure of the positive and propagating feedbacks as a function of the $\bar{u}$ latitude. However, as alluded to in section 6 of Lorenz (2014a), the amplitude of the EOF1 positive feedback and therefore the persistence of EOF1 are too small in the RWC model. For example, the e-folding time scale for EOF1 initial conditions (after the adjustment discussed in section 6) in the RWC model is 22 days compared to 35 days for the GCM (after the transient negative feedback). This discrepancy might be simply due to biases in the RWC because RWC has a tendency to under-predict the response to external forcing even when the full wave activity change is prescribed (see Fig. 5 in Lorenz (2014a)). This discrepancy might also be the result of a positive baroclinic feedback acting with the barotropic feedbacks discussed here (e.g. Barnes and Thompson (2014)). Any theory for the baroclinic feedback, however, should also explain why only EOF1 is

[8] The latitude of the relative minimum in the aK^* is approximately the latitude of the relative maximum in the reflecting level.

associated with a positive feedback.

Acknowledgments.

The author would like to thank Paulo Ceppi, Dan Vimont and three anonymous reviewers for their helpful comments and suggestions on the manuscript. This research was supported by NSF grants ATM-0653795 and AGS-1265182.

REFERENCES

Barnes, E. A. and D. L. Hartmann, 2011: Rossby wave scales, propagation, and the variability of eddy-driven jets. *J. Atmos. Sci.*, **68**, 2893–2908.

Barnes, E. A., D. L. Hartmann, D. M. W. Frierson, and J. Kidston, 2010: Effect of latitude on the persistence of eddy-driven jets. *Geophys. Res. Lett.*, **37**, L11 804.

Barnes, E. A. and D. W. J. Thompson, 2014: Comparing the roles of barotropic versus baroclinic feedbacks in the atmosphere's response to mechanical forcing. *J. Atmos. Sci.*, **71**, 177–194.

Chen, G., I. M. Held, and W. A. Robinson, 2007: Sensitivity of the latitude of the surface westerlies to surface friction. *J. Atmos. Sci.*, **64**, 2899–2915.

Chen, G. and R. A. Plumb, 2009: Quantifying the eddy feedback and the persistence of the zonal index in an idealized atmospheric model. *J. Atmos. Sci.*, **66**, 3707–3720.

Chen, G. and P. Zurita-Gotor, 2008: The tropospheric jet response to prescribed zonal forcing in an idealized atmospheric model. *J. Atmos. Sci.*, **65**, 2254–2271.

Edmon, H. J., B. J. Hoskins, and M. E. McIntyre, 1980: Eliassen-Palm cross sections for the troposphere. *J. Atmos. Sci.*, **37**, 2600–2616.

Feldstein, S. B., 1998: An observational study of the intraseasonal poleward propagation of zonal mean flow anomalies. *J. Atmos. Sci.*, **55**, 2516–2529.

Hartmann, D. L., 1995: A PV view of zonal flow vacillation. *J. Atmos. Sci.*, **52 (14)**, 2561–2576.

Hartmann, D. L. and P. Zuercher, 1998: Response of baroclinic life cycles to barotropic shear. *J. Atmos. Sci.*, **55 (3)**, 297–313.

Held, I. M. and B. J. Hoskins, 1985: Large-scale eddies and the general circulation of the troposphere. *Advances in Geophysics.*, **28**, 3–31.

Held, I. M. and P. Phillips, 1987: Linear and nonlinear barotropic decay on the sphere. *J. Atmos. Sci.*, **44**, 200–207.

Held, I. M. and M. J. Suarez, 1994: A proposal for the intercomparison of the dynamical cores of atmospheric general circulation models. *Bull. Amer. Meteor. Soc.*, **75**, 1825–1830.

James, I. and J. Dodd, 1996: A mechanism for the low-frequency variability of the mid-latitude troposphere. *Quart. J. Roy. Meteor. Soc.*, **122 (533)**, 1197–1210.

Jin, F., L. Pan, and M. Watanabe, 2006a: Dynamics of synoptic eddy and low-frequency flow interaction. Part I: A linear closure. *J. Atmos. Sci.*, **63 (7)**, 1677–1694.

Jin, F., L. Pan, and M. Watanabe, 2006b: Dynamics of synoptic eddy and low-frequency flow interaction. Part II: A theory for low-frequency modes. *J. Atmos. Sci.*, **63 (7)**, 1695–1708.

Kidston, J. and G. K. Vallis, 2012: The relationship between the speed and the latitude of an eddy-driven jet in a stirred barotropic model. *J. Atmos. Sci.*, **69**, 3251–3263.

Kidston, J., G. K. Vallis, S. M. Dean, and J. A. Renwick, 2011: Can the increase in the eddy length scale under global warming cause the poleward shift of the jet streams? *J. Climate*, **24**, 3764–3780.

Lee, S., S.-W. Son, K. Grise, and S. B. Feldstein, 2007: A mechanism for the poleward propagation of zonal mean flow anomalies. *J. Atmos. Sci.*, **64 (3)**, 849–868.

Lorenz, D. J., 2014a: Understanding mid-latitude jet variability and change using Rossby wave chromatography: Methodology. *submitted to J. Atmos. Sci.*

Lorenz, D. J., 2014b: Understanding mid-latitude jet variability and change using Rossby wave chromatography: Poleward shifted jets in response to external forcing. *submitted to J. Atmos. Sci.*

Lorenz, D. J. and D. L. Hartmann, 2001: Eddy-zonal flow feedback in the Southern Hemisphere. *J. Atmos. Sci.*, **58**, 3312–3327.

Lorenz, D. J. and D. L. Hartmann, 2003: Eddy-zonal flow feedback in the Northern Hemisphere winter. *J. Climate*, **16**, 1212–1227.

Randel, W. J. and I. M. Held, 1991: Phase speed spectra of transient eddy fluxes and critical layer absorption. *J. Atmos. Sci.*, **48**, 688–697.

Rivière, G., 2009: Effect of latitudinal variations in low-level baroclinicity on eddy life cycles and upper-tropospheric wave-breaking processes. *J. Atmos. Sci.*, **66 (6)**, 1569–1592.

Robinson, W. A., 1996: Does eddy feedback sustain variability in the zonal index? *J. Atmos. Sci.*, **53 (23)**, 3556–3569.

Robinson, W. A., 2000: A baroclinic mechanism for the eddy feedback on the zonal index. *J. Atmos. Sci.*, **57**, 415–422.

Sparrow, S., M. Blackburn, and J. D. Haigh, 2009: Annular variability and eddy-zonal flow interactions in a simplified atmospheric GCM. Part I: Characterization of high-and low-frequency behavior. *J. Atmos. Sci.*, **66 (10)**, 3075–3094.

Sun, L., G. Chen, and J. Lu, 2013: Sensitivities and mechanisms of the zonal mean atmospheric circulation response to tropical warming. *J. Atmos. Sci.*, **70**, 2487–2504.

Vallis, G. K., E. P. Gerber, P. J. Kushner, and B. A. Cash, 2004: A mechanism and simple dynamical model of the North Atlantic Oscillation and annular modes. *J. Atmos. Sci.*, **61**, 264–280.

Zhang, Y., X.-Q. Yang, Y. Nie, and G. Chen, 2012: Annular mode-like variation in a multilayer quasigeostrophic model. *J. Atmos. Sci.*, **69 (10)**, 2940–2958.